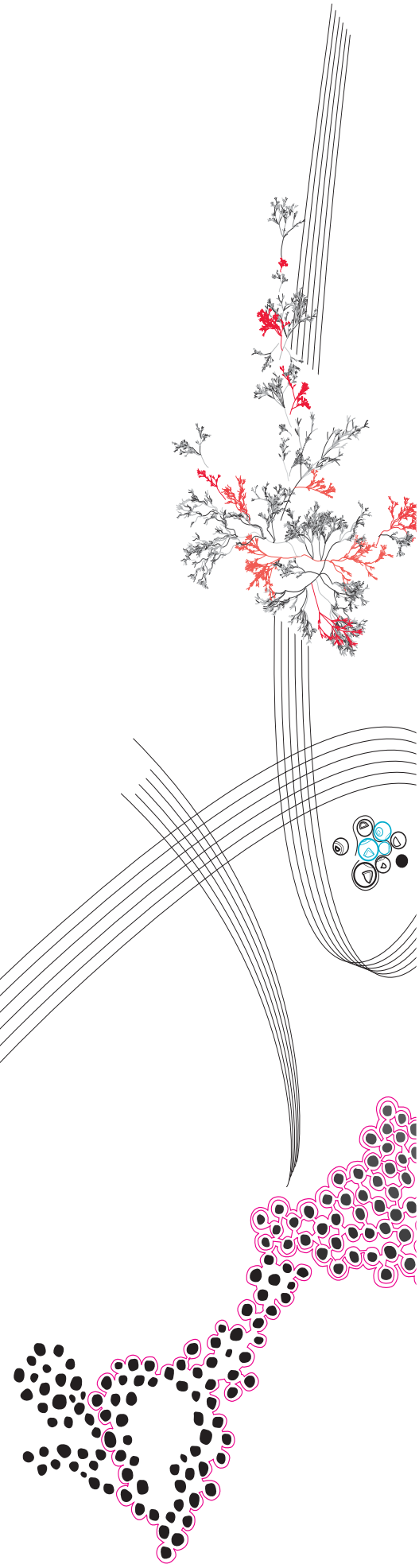

UNIVERSITY OF TWENTE

BACHELOR ASSIGNMENT
AT DEVELOPMENTAL BIOENGINEERING (DBE)

VHH-Mediated targeting of osteoarthritic Synovium by synthesizing functional lipid nanoparticles using post-insertion

C.M. van Mourik (s2857219)
July 10, 2024

main supervisor:
Prof.Dr. H.B.J. Karperien

Daily supervisors:
Dr. J. Hendriks and Dr. B. Zoetebier

External supervisor:
Dr. R. Bansal

Abstract

Osteoarthritis is the most common type of arthritis and one of the primary causes of disability worldwide. This disease is characterized by synovitis, the inflammation of the synovial membrane of the joint. The inflamed membrane secretes catabolic and pro-inflammatory products, this results in an imbalance between M1(pro-inflammatory) and M2(anti-inflammatory) macrophages. The imbalance eventually causes cartilage degradation in the joint. It is a chronic disease with no effective treatments so far. A potential treatment option is to use targeted drug delivery. In this way, drugs can be transported to specific target cells. Using siRNA as the drug has proven to be effective. The drugs will inhibit M1 or activate M2 macrophages. For the transport and encapsulation of the drugs, ionizable lipid nanoparticles (LNPs) can be used. LNPs are neutral at physiological pH in the body but become cationic when a low pH is reached in cells. Resulting in the breakdown of the LNP and the release of its content. To target specific types of macrophages, the LNPs need to be coated with biological ligands. For this, VHHs show promise to be used since they are small antibody fragments of approximately 15 kDa with the same binding affinity as monoclonal antibodies. This thesis focuses on the synthesis of the functional LNPs. The method of post-insertion of lipids is tested, and thereby, the lipids are first conjugated to the functional biological ligand. After conjugation, the functional lipid is inserted into the LNP, for this, three molar ratios of lipids are tested: 0.1, 0.2 and 0.3%. The biological ligand in this report is first a fluorescent Cy3 dye to confirm conjugation, and later a VHH that targets IL-1R receptors on cells. Two reactive groups, DBCO and Maleimide, and two PEG spacer lengths, 2000 and 5000 Da, are tested for the lipids. LNPs are successfully synthesized with mCherry and tRNA as drugs, with the help of a microfluidic chip with a herringbone structure. The conjugation of the lipids(DSPE-PEG-Mal/DBCO) to the Cy3-PEG-SH/Azide-PEG2000-Cy3 dye is analyzed with fluorescence measurements and confirmed for both reactive groups and PEG spacers. A higher conjugation is achieved with the 5000 Da PEG spacers than the 2000 Da PEG spacers. The conjugation of DSPE-PEG-Mal to VHH with a 5000 Da PEG spacer is confirmed by a quantification by SDS-page. The post-insertion of DSPE-PEG-Mal-Cy3 and DSPE-PEG-Mal-VHH showed inconclusive results. The post-insertion of DSPE-PEG-DBCO-Cy3 succeeded for both PEG spacers, analyzed by fluorescence measurements. A higher molar ratio of DSPE-PEG-DBCO-Cy3 leads to a higher fluorescence signal, so more lipids are inserted into the LNPs. DSPE-PEG-DBCO-Cy3 with 5000 Da PEG has a higher fluorescence than with 2000 Da PEG, so more lipids are inserted into the LNPs. All post-inserted LNPs are measured on size and PDI with DLS. Post-insertion leads to a higher size and PDI of the LNPs, a higher molar ratio does not influence the size and PDI.

Contents

1 Introduction **3**
- 1.1 Osteoarthritis (OA) . . . 3
- 1.2 Targeted drug delivery . . . 4
- 1.3 Possible treatment OA . . . 4
- 1.4 Post-insertion . . . 4
- 1.5 Assignment aim . . . 5
- 1.6 Future project aim . . . 6

2 Theoretical background **7**
- 2.1 Targeted drug delivery . . . 7
  - 2.1.1 Small interfering RNA (siRNA) . . . 7
  - 2.1.2 Messenger RNA (mRNA) . . . 7
  - 2.1.3 Micro RNA (miRNA) . . . 7
- 2.2 Nanoparticles (NPs) . . . 8
  - 2.2.1 Nanoparticle properties . . . 8
  - 2.2.2 Lipid nanoparticle production techniques . . . 8
- 2.3 Lipid nanoparticles (LNP) . . . 10
  - 2.3.1 Liposomes . . . 12
  - 2.3.2 Solid lipid nanoparticles (SLN) . . . 12
  - 2.3.3 Nanostructured lipid carriers (NLC) . . . 12
  - 2.3.4 Lipid drug conjugates (LDC) . . . 12
  - 2.3.5 Lipid nanocapsules (LNC) . . . 13
- 2.4 Targeting . . . 13
  - 2.4.1 Antibodies . . . 13
  - 2.4.2 Peptides and proteins . . . 14
  - 2.4.3 Polysaccharides . . . 14
  - 2.4.4 Aptamers . . . 14
  - 2.4.5 VHH . . . 14
- 2.5 Conjugation techniques . . . 15
  - 2.5.1 Electrostatic and hydrophobic interactions . . . 15
  - 2.5.2 Host-Guest interactions . . . 16
  - 2.5.3 Click-chemistry . . . 16
- 2.6 Techniques for LNP characterization and conjugation efficiency . . . 17
  - 2.6.1 Dynamic light scattering (DLS) . . . 17
  - 2.6.2 Scanning electron microscope (SEM) . . . 17
  - 2.6.3 SDS-page . . . 17
  - 2.6.4 Western-blot . . . 18

3 Materials and methods **19**
- 3.1 Materials . . . 19
- 3.2 Methods . . . 19
  - 3.2.1 LNPs fabrication . . . 19

3.2.2 Synthesis of an Azide functional Cy3 dye . . . 20
3.2.3 Conjugation of lipids to Cy3 dyes . . . 20
3.2.4 Conjugation of lipids to VHHs . . . 21
3.2.5 Post-insertion . . . 22
3.3 Analysis . . . 23
3.3.1 Azide functional Cy3 dye . . . 23
3.3.2 Conjugation lipids-Cy3 . . . 23
3.3.3 Conjugation lipids-VHH . . . 23
3.3.4 Post-insertion . . . 24

4 Results and discussion **25**
4.1 LNPs fabrication . . . 25
4.2 Conjugation DSPE-PEG-DBCO to Azide-PEG2000-Cy3 dye . . . 25
4.3 Conjugation DSPE-PEG-Mal to Cy3-PEG-SH dye . . . 27
4.4 Post-insertion DSPE-PEG-DBCO/Mal-Cy3 . . . 29
4.4.1 Post-insertion DSPE-PEG-DBCO-Cy3 Batch 2 . . . 29
4.4.2 Post-insertion DSPE-PEG-DBCO-Cy3 Batch 3 . . . 32
4.5 Conjugation DSPE-PEG-Mal to VHH . . . 36
4.5.1 Batch 1 . . . 36
4.5.2 Batch 2 . . . 37
4.6 Post-insertion DSPE-PEG-Mal-VHH . . . 39

5 Conclusion **43**

6 Acknowledgements **44**

References **44**

A Inconclusive results **50**
A.1 Post-insertion DSPE-PEG-Mal-Cy3 . . . 50
A.2 Post-insertion DSPE-PEG-DBCO-Cy3 batch 1 . . . 52

Chapter 1

Introduction

1.1 Osteoarthritis (OA)

Osteoarthritis (OA) is the most common type of arthritis and one of the primary causes of disability worldwide [1]. Arthritis is a group of diseases characterized by inflammation and degeneration of the joints, with osteoarthritis specifically involving the degeneration of cartilage. The most common type of OA is knee-OA because this is the largest synovial joint in the human body. According to the GBD 2021 Osteoarthritis Collaborators, 7.6% of the global population had OA in 2020, and it is expected to grow to 74.9% for knee OA, the prevalence is higher for adults above 65 years old [2]. Common risk factors for OA are age, obesity, trauma and mechanical loading. It is a chronic disease and has no effective treatments to delay the disease progression and reduce the symptoms. In an OA joint, the synovial membrane is inflamed, this is also called synovitis. The membrane produces catabolic products and pro-inflammatory macrophages (M1). The balance between M1 and M2 (anti-inflammatory) macrophages is disrupted. This will eventually result in the degeneration of the joint cartilage, as seen in figure 1.1. This is a big problem because the cartilage is responsible for the absorption and distribution of the mechanical load. The inflammation will result in swelling, pain and stiffness around the joint. All these symptoms eventually result in chronic pain and loss of mobility, which lowers the quality of life [3, 4].

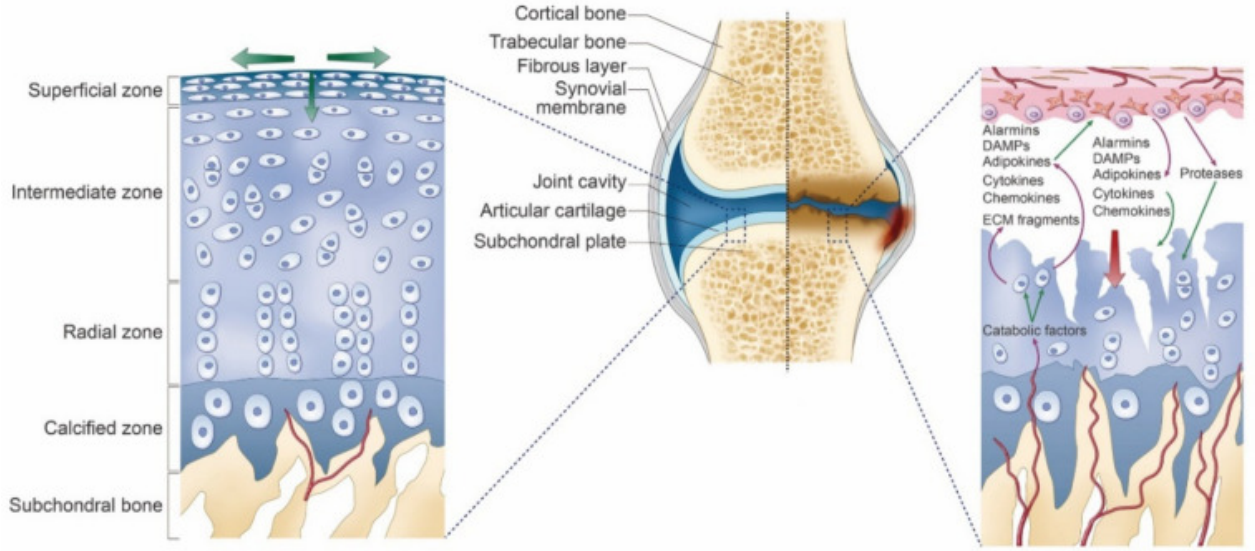

Figure 1.1: Schematic overview of an OA joint. Healthy cartilage on the left, with an absence of vessels in the cartilage. OA cartilage on the right, with vessels in the cartilage and degradation of cartilage [4].

1.2 Targeted drug delivery

Most often, the disease site is distant from the site where the drug is administered. For this problem, targeted drug delivery is a promising solution. Targeted drug delivery is the transport system of a pharmaceutical (drug) to its targeted area, this can be on organ, cellular or tissue level. After arriving at the targeted area, the pharmaceutical will achieve the desired therapeutic effect [5]. To achieve the needed therapeutic effect, drug carriers are loaded with the correct genetic material. It was proven that loading the particles with RNA results in an efficient payload for nanoparticles. Different types of RNA can be used for targeted drug delivery, such as siRNA, miRNA and mRNA [6].

Nanotechnology is a relatively new field, it is rapidly growing and shows a lot of promise to be used in targeted drug delivery. Nanoparticles (NPs) can be used as carriers to deliver specific drugs to the targeted area [7]. The NPs can mimic and alter biological processes due to their nanometer size, which is the same size range of biomolecules in the human body [8]. NPs can be designed with specific surface properties, resulting in only targeting the diseased cells and avoiding the healthy cells. They can release their drugs in a controllable manner over time and quantity [7].

1.3 Possible treatment OA

To find a treatment for OA, one possible solution is to restore the balance between M1 and M2 macrophages. This can be done by inhibiting M1 or activating M2 macrophages using specific drugs (RNA/DNA sequences). For the transport of the drugs, nanoparticles can be used. One type of nanoparticle is lipid nanoparticles (LNPs). These are nanoparticles that consist of lipids, lipids are molecules with a hydrophilic head linked to their hydrophobic fatty acid chain [9]. LNPs will be used as drug carriers due to their stability, regulated drug release, bio-compatibility, bio-functionalization and the changeability of the lipid matrix. A challenge in this field is bringing the negatively charged LNP over the cell membrane. Wu L. Et al. have shown that LNPs succeeded in performing this and they are adequate drug carriers in the human body [10]. The LNP will encapsulate the DNA/RNA because of electrostatic interactions with DNA/RNA. LNPs are neutral at physiological pH, but become cationic because of the low pH in endosomes. This causes the cell to break down the LNP and the LNPs release their content [11]. To get the LNPs to the target cells, biological ligands can be conjugated on the outside of the LNP. VHHs are a perfect candidate to function as biological ligands. Because of their good properties, such as their high affinity, specificity, low immunogenicity and small size ($\sim$15kDa). Another reason is the variety of VHHs which can be easily produced for different targets. In this research, the VHHs target the IL-1R cell receptor.

1.4 Post-insertion

The LNPs need to have reactive groups at the surface to be able to react with biological ligands for the targeting of specific disease sites. Usually, the lipids with the reactive groups are put in simultaneously with the other lipids for the LNP fabrication. L.E. Swart. et al. showed that post-insertion of the lipid ligands into preformed LNPs is more favorable than direct-surface modification because it retains the physicochemical properties and morphology of the LNPs [12]. They successfully proposed a protocol to insert lipids with fluorescent or targeting ligands into the LNPs. In this technique, the hydrophobic tails of the lipid are spontaneously inserted into the lipid bilayer of the LNP. Figure 1.2 shows a schematic overview of two types of post-insertion: DSPE-PEG-DBCO post-insertion, followed by SPAAC to couple an Azide functional component. And the post-insertion of the preformed coupled DSPE-PEG-DBCO to an Azide component.

The timing of the post-insertion is an important parameter. Applying the post-insertion after the dialysis of the LNPs shows the hydrodynamic diameter increasing the least. The PDI also has the smallest increase after dialysis. Post-insertion occurred quickly and with a high efficacy across a broad range of temperatures [12].

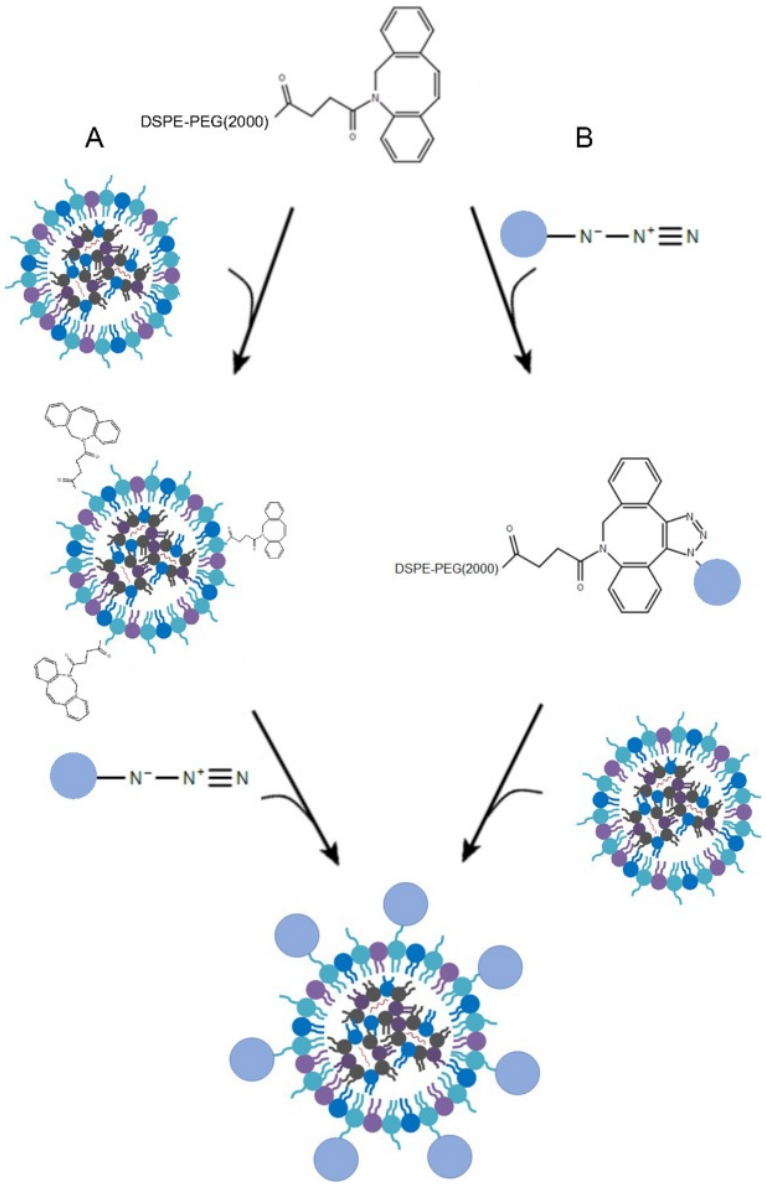

Figure 1.2: Schematic overview of two types of post insertion. (A) DSPE-PEG-DBCO post-insertion, followed by SPAAC to couple an Azide functional component. (B) Post-insertion of the preformed coupled DSPE-PEG-DBCO to an Azide component [12].

1.5 Assignment aim

This study aims to synthesize (fluorescently) labeled LNPs that can be used for targeted delivery using VHHs. The LNPs will be fabricated using a microfluidic chip with a herringbone structure. The use of a microfluidic chip will result in smaller and more monodisperse nanoparticles. Figure 1.3 shows a schematic overview of the desired LNP, with the associated molar ratios of the various lipids. The Onpattro formulation of the LNPs is used, since the effectiveness of this formulation has been confirmed [13]. VHHs will be used as biological ligands on the LNP.

Post-insertion will be researched to couple the biological ligands to the LNPs because it shows a lot of promise by keeping the PDI low and minimally increasing the size of the LNPs. For post-insertion, the lipids need to be conjugated to the biological ligand first. To test if the conjugation works properly, the lipids are first conjugated to Cy3(fluorescent dye) and eventually coupled to VHH.

For the conjugation of the lipids to Cy3/VHH, two reactive groups on the lipids will be tested: dibenzo-

cyclooctyne (DBCO) and Maleimide (Mal). These groups are both reacting by click-chemistry. This is a fast reaction, that leads to a strong and stable bond. This kind of chemistry has already been widely used for the conjugation of biological ligands [14]. The maleimide group on the lipid can react with a thiol group present on the Cy3 or VHH. The DBCO group on the lipid can react with an Azide, to conjugate to the Cy3/VHH a linker needs to be added. This linker is an Azide-functional molecule that can be coupled to the thiol group of the Cy3 and VHH molecules. Also, two PEG lengths of 2000 and 5000 Da will be researched.

Post-insertion will be performed after dialysis of the LNPs, with lipids-DBCO-Cy3, lipid-Mal-Cy3 and lipid-Mal-VHH. The LNPs will be characterized by size and Polydispersity Index (PDI) using DLS. The conjugation of the DBCO/Maleimide to Cy3 will be quantified using fluorescence, and the conjugation of lipid-M aleimide to VHH will be quantified using SDS-page.

This leads to the research question: ***What is the effectiveness of post-insertion for incorporating Cy3 and VHH conjugated lipids into lipid nanoparticles?***

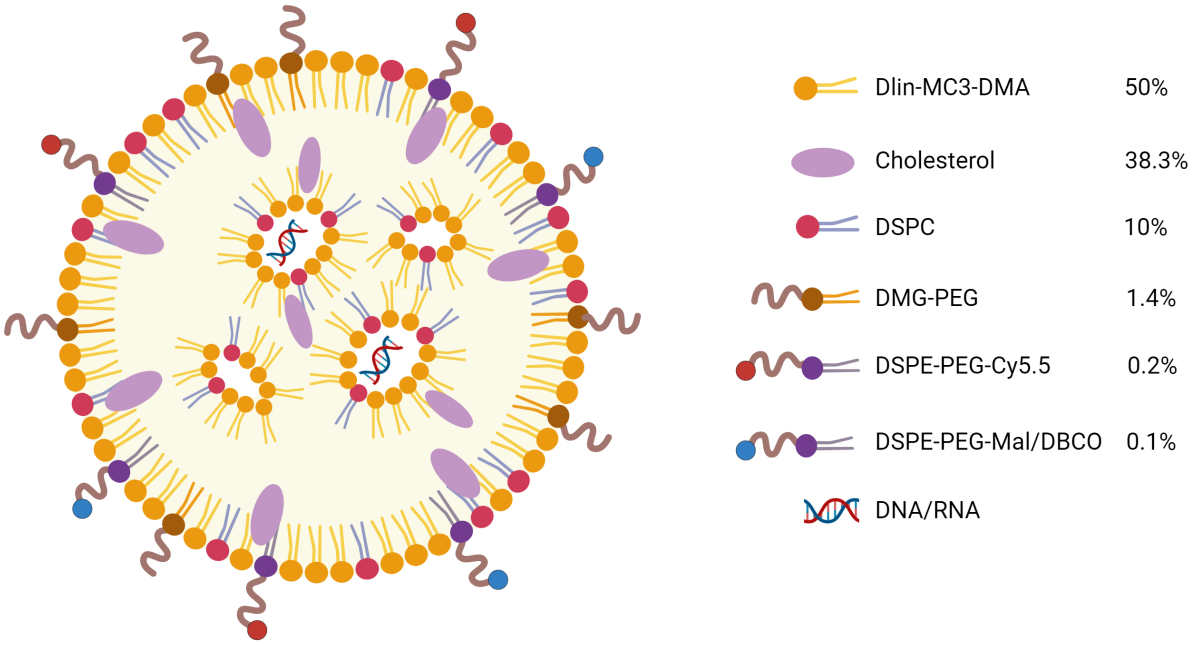

Figure 1.3: Schematic representation of the LNP with the molar ratios of the lipid components.

1.6 Future project aim

To use the LNPs in targeted drug delivery to cure OA, their properties need to be optimized. The future aim is to use siRNA-loaded LNPs, inject them into the body, and target them to the synovial membrane of a joint with OA. There the LNP will fall apart and the siRNA will perform its function. It will inhibit M1 or activate M2 macrophages. VHHs will be used as biological ligands due to their high affinity towards inflammatory macrophages, which are the main players in joint inflammation and pain in the synovial membrane. The uptake of these LNPs in the inflammatory macrophages will counteract the inflammation and reduce the associated pain.

Chapter 2

Theoretical background

2.1 Targeted drug delivery

Targeted drug delivery is the transport system to bring a drug to its target area, this can be on organ, cellular or tissue level. After arriving at the target area, the pharmaceutical will achieve the desired therapeutic effect. The possible cytotoxic effects of the drug are overcome by using targeted delivery, and smaller amounts of drugs are required for the same efficiency [5]. For a successful drug delivery, various aspects need to be considered. The drug encapsulation into the NP, the biofunctionalization of the NPs with targeting ligands on the surface to reach the target area, the binding and uptake of the NPs into the target cells and eventually the drug release [8].

To achieve the desired therapeutic effect, drug carriers need to be loaded with the correct genetic material. It was proven that loading the particles with RNA results in an efficient payload for nanoparticles. Different types of RNA can be used for targeted drug delivery, such as siRNA, miRNA and mRNA [6].

2.1.1 Small interfering RNA (siRNA)

Small interfering RNA (siRNA) is a double-stranded RNA macromolecule consisting of 21 to 23 nucleotides, it has a molecular weight of 13-15 kDa and is negatively charged. This molecule is effective at the post-transcriptional level and helps with gene silencing. In the cytoplasm of the cell, siRNA helps form an RNA-induced silencing complex (RISC). The RISC helps with the silencing of the mRNAs of interest by degrading. However, a disadvantage of the use of siRNA is the poor membrane permeation. This means that for in vivo targeted drug delivery, the particles need to deliver the siRNA into the cytoplasm of the cells. siRNA can also be degraded by nucleases or end up in endosomal traps, which results in non-successful targeted drug delivery [15, 16].

2.1.2 Messenger RNA (mRNA)

mRNA is a large negatively charged single-stranded molecule of 300-1500 kDa [17]. It controls protein synthesis and contains genetic information. A mRNA molecule has a 5'and 3' UTR end, these are the untranslated regions that regulate the translation. It also has a 5'cap, which protects nucleases And a polyA-tail with a length between 30–70 nucleotides, which influences the translation. For example, mRNA used for drug delivery can encode various antigens that fight against tumors or viruses. In the targeted cell, the mRNA carries out its function and is translated into proteins [18]. The large size of the mRNA can cause more problems to encapsulate, compared to siRNA and miRNA [17].

2.1.3 Micro RNA (miRNA)

miRNAs are molecules that regulate gene expression at the post-transcriptional level. They are single-stranded, non-coding RNA molecules with an average length of 22 nucleotides. Most often, miRNAs bind to the 3'UTR (untranslated regions) of the mRNA of interest to suppress the expression. Another option

is the binding of the miRNAs to the 5'UTR. A single miRNA has the possibility to promote and suppress numerous mRNAs at the same time, whereas siRNA and mRNA can only suppress or promote one specific mRNA. This can also be seen as a disadvantage. The miRNA can interact with many targets, which makes it challenging to target specific cells, which could lead to side effects [18, 19, 20].

2.2 Nanoparticles (NPs)

As said before, NPs show promise to be used for targeted drug delivery systems. NPs reach disease sites that are usually inaccessible and reduce the administration frequency [8]. The characteristics of the NP determine their behavior and if the NP can be used as a carrier for targeted drug delivery. NPs for biomedical applications have an ideal size range of 1-200 nm [21]. NPs can undergo surface modification, to achieve better surface properties. For example, polyethylene glycol (PEG) can be added. This minimizes non-specific protein adsorption, which reduces NP uptake by phagocytes and decreases the accumulation in non-targeted organs and makes the NPs more stable [22].

NPs have several advantages over traditional drug-ligand conjugates. NPs have a large number of ligands on the surface and their usage increases the probability of binding to the target, this however depends on the size of the NP and the drug. NPs also have efficient drug loading and high drug payloads within the NPs and can be delivered to specific targets where the ligand interacts with the receptor [8].

There are three types of NPs: polymer-based, lipid-based and non-polymeric NPs [22]. Polymer-based NPs are for example, micelles, protein nanoparticles or nanogels. These NPs have a very high stability, but have a low cell interaction because of the limited affinity for the cell membrane and the poor biocompatibility [23]. Lipid-based NPs are for example, liposomes and exosomes. They have high biocompatibility and can encapsulate a variety of drugs [23]. Non-polymeric NPs are for example, carbon nanotubes, metallic NPs or quantum dots.

2.2.1 Nanoparticle properties

The shape, size, surface area and surface chemistry need to be optimized for a successful drug delivery. The shape and size of the NPs are determined during the synthesis. NPs have a high surface-to-volume ratio, with an optimal size range between 20-200 nm. NP smaller than 10 nm can be removed by kidney filtration, and NPs bigger than 200 nm can be cleared by phagocytes [22]. The charge of the NP is also an important factor. Particles of at least $\pm$20mV are desired for electrostatic and sterically stable particles [24]. NPs with a charge between -10 mV and +10 mV are less prone to non-specific interactions [22]. The NP charge is related to the pH sensibility of the NPs. They can be designed to target specific cells dependent on pH [22]. The charge of the NPs is also related to cellular interactions. NPs with a negative surface charge are repelled from the negatively charged cell membrane. Positively charged NPs can interact better with the cells, but are more toxic to the cells compared to neutral or anionic particles [25, 26]. NPs with a hydrophilic coating prevent opsonization and improve the circulation time of the NPs [8]. NPs should have a low Polydispersity Index (PDI), so monodisperse, to ensure a consistent drug release rate [27]. Summarizing, NPs should be biocompatible, non-immunogenic, non-inflammatory, biodegradable, non-toxic and stable. All these properties will improve the targeted drug delivery [8, 27].

2.2.2 Lipid nanoparticle production techniques

There are multiple techniques to synthesize LNPs. The advantages and disadvantages are explained in the following section, as well as the mechanism of the technique. Table 2.1 shows an overview of the advantages and disadvantages of the different techniques.

Thin-film hydration

Firstly, thin-film hydration is one of the most common techniques used for the production of LNPs. It is a passive encapsulation method where the phospholipids self-assemble spontaneously into vesicles. It is a simple and cheap method. The lipids are in an organic solvent (ethanol or chloroform), after the LNP formation the solvent is evaporated, which results in a thin lipid layer. This layer is hydrated using a buffer solution with nucleic acids. The hydrophobic and hydrophilic parts self-assemble and result in large multilamellar vesicles in micrometer size and considerable heterogeneity [28].

Ethanol injection

Another method to make LNPs is ethanol injection, which is an alternative to thin-film hydration. It is a simple technique with no use of sonication. The dissolved lipids in ethanol are injected under stirring into an aqueous buffer at a fast rate. The buffer has a higher volume than the lipid solution and contains the drug for encapsulation. This forms the vesicles rapidly. The sizes of the LNPs are controllable by adjusting the lipid concentration, stirring and injection rate and the types of lipids. However, this easy technique has a shortage in reproducibility, scalability and encapsulation efficiency. For this, T-junction mixing and microfluidic mixing are introduced [28].

T-junction mixing

T-junction mixing can create nucleic acid-loaded nanoparticles. It is reproducible and controllable, so appropriate for large batches. It has a higher encapsulation efficiency than conventional methods to create LNPs. Two different solvents are injected into a T-junction, this causes rapid mixing due to collision and a turbulent flow. It is crucial to keep the speed of the mixture constant. The mixing will encapsulate the RNA and will create LNPs. The flow rate influences the size and PDI of the particles. The size decreases with an increase in the total flow rate. A higher flow rate will result in a lower PDI. However, a short mixing time can lead to aggregation and more heterogeneous LNPs [28].

Microfluidic mixing

Lastly, microfluidic mixing can be used. It uses a microfluidic chip and creates smaller and more monodisperse LNPs compared to the other techniques. The channels have a laminar flow, which results in slow molecular diffusion. A staggered-herringbone structure is implemented in the chip channels, promoting the reduction of hydrodynamic dispersion and allowing effective solution mixing. The structure causes rapid mixing, which results in supersaturation and the formation of LNPs. Using a microfluidic chip improves the control of the particle size and PDI and has a higher encapsulation. The size and size distribution of the LNPs can be influenced by adjusting the total flow rate and the flow rate ratio. By using a higher total flow rate, smaller LNPs will be formed [28].

Table 2.1: Comparison of multiple LNP production methods [28].

LNP production methods	Advantages	Disadvantages
Thin-film hydration	- Simple procedure - No expensive, complicated equipment needed	- Formulation of large multilamellar vesicles - Heterogeneous in size - Low encapsulation efficiency - Time consuming - Large-scale production difficulty
Ethanol injection	- Simple procedure - Size controllable	- Time consuming - Low encapsulation efficiency
T-junction mixing	- Reproducible & size controllable - Uniform particle formulation - Large-scale production - High encapsulation efficiency	- Lab-scale not preferred - Relatively high flow rate required
Microfluidic mixing	- Reproducible & size controllable - Uniform particle formulation - High encapsulation efficiency - Easily scalable	- Possible clogging in micro channel

2.3 Lipid nanoparticles (LNP)

Lipid nanoparticles consist of lipids, which are molecules with a hydrophilic head linked to a hydrophobic fatty acids chain [9]. A classic LNP formulation consists of ionizable cationic lipids, helper lipids, cholesterol and PEG-lipids. The chemical structures of the lipids can be seen in figure 2.1. The ionizable cationic lipids add up to around 50% of the lipids of the LNP. A common example is DLin-MC3-DMA, a tertiary amine with hydrophobic tails. Helper lipids make up 10% of the lipids. DOPE is a helper lipid that is mostly used in vivo and DSPC is mostly used in vitro because of an increased transfection efficiency. Cholesterol adds up to 30-40% of the lipids, maintaining the rigid form of the LNP. The PEG-lipids make up 1-5% of the total lipids, this makes the particle smaller because of the localization at the surface [6]. The optimal size of a LNP is 20-200 nm, to make them resist the fluid flow to cross the interstitium [9].

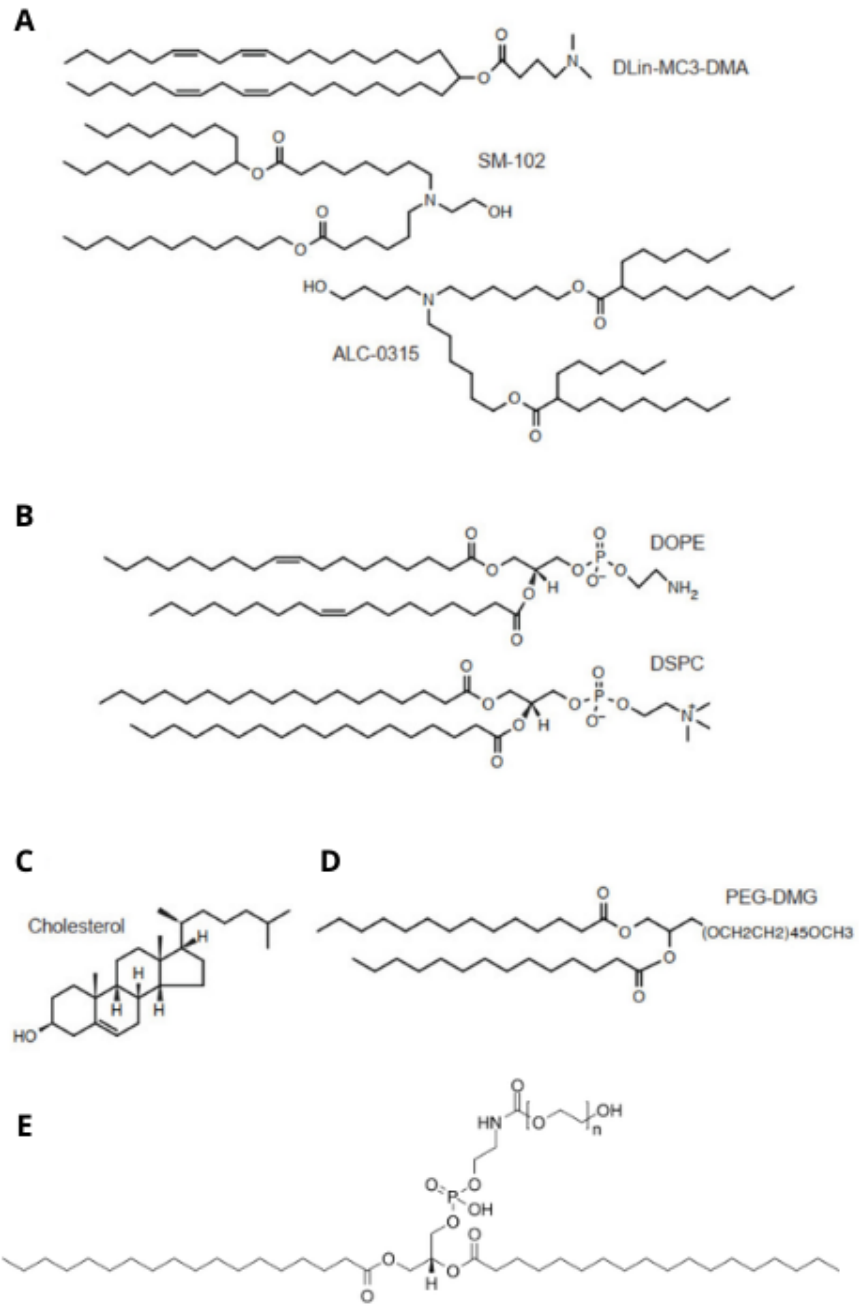

Figure 2.1: Chemical structures of various lipids for LNPs. (A) DLin-MC3-DMA, SM-102, and ALC-0315. (B) DOPE and DSPC. (C) Cholesterol. (D) PEG-DMG. (E) DSPE-PEG2000 [6, 29].

LNPs are widely used in targeted drug delivery due to their characteristics. They can transport both hydrophilic and hydrophobic drugs, have low or no toxicity[30] and are very stable [31]. LNPs also have a regulated drug release and an extended lifetime. LNPs can eventually be functionalized with biological ligands for active targeting [30]. So the main advantages are the interchangeability of the building blocks of the LNP, and the biocompatibility of the lipid matrix [31, 32].

There are five different types of LNPs, liposomes, solid nanoparticles, nanostructured lipid carriers, lipid drug conjugates and lipid nanocapsules. They differ in the way they carry the drugs and in their composition [31].

2.3.1 Liposomes

Liposomes are the early generation of lipid-based NPs. Liposomes are made out of lipids and are in the nanometer size. Liposomes consist of an internal aqueous core with an amphipathic phospholipid bilayer. It can encapsulate hydrophobic drugs in the lipid bilayers and hydrophilic drugs in the core [11]. The lipid bilayer vesicles are spontaneously formed in water. Shortly after, the potential for drug delivery was acknowledged. Liposomes are used as drugs and vaccines. For example, cancer drugs have a low solubility in water, so liposomes could be used to encapsulate these drugs. The first accepted liposomal drug is Doxil, which is used for cancer treatment. Currently, there are many liposomal drugs on the market. However, they have complex production methods, difficult large-scale production and have a low efficiency in entrapping the drugs [33].

2.3.2 Solid lipid nanoparticles (SLN)

Solid lipid NPs are spherical NPs consisting of structured solid lipids, containing the drug molecules in the core. They also have a surfactant layer to stabilize the SLN in an aqueous phase [34]. SLNs combine the advantages of polymeric NPs and liposomes. They have a size range of 40-1000 nm, are non-toxic and biodegradable. Various amounts of surfactants are responsible for the stability of the particle, ranging from 0.5-5% [35]. SLNs have improved drug stability, because of the solid matrix. Both hydrophobic and hydrophilic drugs can be encapsulated, and SLNs have a higher entrapment efficiency compared to liposomes. By changing the lipid components, the drug release can be controlled. However, SLNs have a low drug loading capacity and a low long-term drug retention [11].

2.3.3 Nanostructured lipid carriers (NLC)

Nanostructured lipid carriers are the successor of the SLNs. They are made out of solid and liquid lipids and emulsifiers, the ratio between them determines the entrapment efficiency and stability of the NLCs. Emulsifiers stabilize the NPs. The structural defects in solid lipids result in an amorphous or imperfect structure. Which provides a high drug load, because of the prevention of drug leakage [34]. NLCs have multiple advantages, such as a high loading capacity and reduced or absent evaporation of the drug during storage. They are non-toxic and biodegradable. NLCs allow more drug accommodation, due to the presence of spatial lipids like glycerides in the lipid matrix of the NP. However, NLCs also have disadvantages. They can be cytotoxic and have low stability [35]. The low solubility of the drugs inside the solid lipids results in a low drug encapsulation efficiency of the NLCs [11]. NLCs have been used in clinical trials for example, for COVID-19 mRNA [36].

2.3.4 Lipid drug conjugates (LDC)

Lipid drug conjugates were developed to achieve a better drug loading capacity for hydrophilic drugs than SLNs and NLCs [31]. LDCs have been modified with lipids using covalent bindings. They have multiple advantages compared to the other LNP types like lower toxicity and improved drug loading. Different strategies can be used for the conjugation. Firstly, fatty acids can be used. The carboxyl end of the lipid reacts with the amine or hydroxyl group of the drug and forms an ester or amide link. Another option is to conjugate the drugs with steroids, for example, cholesterol or cholic acid derivatives. Steroids have a 4-ringed structure, the hydroxyl group of the steroids reacts with the drug and forms a covalent bond. This conjugation lowers side effects and makes the cellular uptake more efficient. The third option is to conjugate the drugs with glycerides. A glycerol is combined with three fatty acids by ester bonds, one fatty acid chain is replaced by the drug. Most often, the middle chain is replaced, because it takes advantage of the pathways in the human body where hydrolyzation takes place, this reaction results in free fatty acids. The free fatty acids accumulate in the lymphatic system, improving drug absorption by using the lymphatic transport system of the human body. The last option is to conjugate the drugs with phospholipids. This can be done by linking the drug molecule to the phosphate group, creating a phosphoester, by attaching the drug molecule on the hydroxyl group at the sn2 position. This improves the encapsulation of the drugs into lipid-based drug delivery systems [37].

For the conjugation, various chemical bonds can be formed. The most common bonds are the ester bond, amide bond, hydrazone bond and disulfide bond. An ester bond is the reaction between a hydroxyl group and a carboxylic group. Amide bonds form by the reaction of a carboxylic group with an amine group. Hydrazone bonds form by a reaction of hydrazine with a carboxylic group, the O is replaced with a NNH2 group. Hydrazone bonds are acidic-labile, the bond gets destroyed when in an acidic environment of cells. They are used to make pH-dependent LNPs [38]. Disulfide bonds are bonds between two sulfur atoms for example, in cysteine [39]. These bonds are stable and will be cleaved by enzymes after cellular uptake [37].

2.3.5 Lipid nanocapsules (LNC)

Lipid nanocapsules have a core-shell structure. They have an internal liquid or semi-liquid oil core and an external lipid layer that creates a tensioactive cohesive membrane around the oily core, which is solid at room temperature and stabilizes the particle [31, 40]. LNCs are a combination of liposomes and polymeric nanocapsules and have a physical stability of more than 18 months. LNCs can be made smaller than 100 nm and with monodispersity [41]. They can encapsulate a wide variety of drugs, such as hydrophilic, hydrophobic and lipophilic drugs. LNCs can contain target-specific patterns on the surface, which could be used for targeted drug delivery [42]. The drug loading can induce changes in the structure of the particle, which can affect the drug loading efficiency. This can eventually have an advantage, which leads to a higher drug loading and longer drug release [40].

2.4 Targeting

The performance of the drug delivery system depends on the targeting of the NP to the disease site, the drug carriers need to have specific ligands to interact with specific cells. There are two types of targeting, namely active and passive targeting. Passive targeting relies on the physicochemical properties of the particles, it uses the natural, physiological uptake mechanisms of the human body [43]. Passive targeting is based on the accumulation of drugs at the targeted areas, NPs enter blood vessels and are more directed towards the blood vessels at the disease site [5]. For example, NPs can target tumors due to the enhanced permeation and retention (EPR) effect. Active targeting is based on the biological interaction between the cell target and the ligands on the NP surface, for this biological ligands can be used. These ligands bind to specific receptors on the surface of the cell. Otherwise, the drug carriers will interact with non-targeted tissues or cells and cause side effects. Examples of biological ligands are antibodies, peptides, proteins, polysaccharides, aptamers and VHHs. The ligands can be functionalized on the NPs in two ways, via chemical conjugation or physical adsorption [8, 43].

2.4.1 Antibodies

Antibodies (Ab) are also known as immunoglobulins (Igs) and can be used as biological ligands. They are the most commonly used biological ligands. They are big molecules of $\sim$150 kDa and are favorable for targeting due to their high specificity. However, Abs can be immunogenic and because of their size, the antibody density on the NP surface is limited [43]. Antibodies are mostly extracted from animals. However, there is an animal-to-animal difference in the same antibody, which can interfere with the binding.

Antibodies are Y-shaped proteins that have two light and two heavy chains and have a variable region that can bind to various antigens or receptors on cells. The configuration of the antibody plays an important role in the design of the conjugated NPs, this will affect the in vivo efficiency of the targeted drug delivery system.

Antibodies targeting epithelial growth factor receptors (EGFR) and anti-vascular endothelial growth factor (VEGF) are the most commonly used antibodies for targeted drug delivery. Both are overexpressed in tumor epithelial cells and therefore excellent targets to epithelial cells [44].

2.4.2 Peptides and proteins

Peptides are short chains of 40 or fewer amino acids, they are the building blocks for proteins with a molecular weight less than 5000 Da. Proteins are large molecules that exist out of 50 or more amino acids, starting at a molecular weight of 5000 Da [45, 46]. Both molecules are linked by peptide bonds and can be used for targeting. The peptides are the binding regions of the interested target. They have multiple advantages such as low or non-immunogenicity, good stability, low production costs and easy conjugation to the NP surface with a high density due to their small size. However, peptides have a higher chance of non-specific binding, lower binding affinity and proteolytic cleavage.

The most commonly used peptide is the tripeptide arginine–glycine–aspartate (RGD) peptide. The RGD binds to integrins, which are overexpressed in the endothelial cells of tumor tissue. Because of this, it is a well-known target peptide for tumors [43].

2.4.3 Polysaccharides

Polysaccharides are carbohydrates that exist out of more than ten monosaccharide units linked by a glycosidic bond. The molecular weights of polysaccharides can vary widely depending on their type and length of polysaccharide chain. Natural polysaccharides are biocompatible, non-toxic, stable and have an affinity towards specific receptors. Which makes them an excellent candidate as biological ligands [47]. For example, hyaluronic acid (HA) is a common polysaccharide. It is a major component of the extracellular matrix (ECM). CD44, which is overexpressed in cancer cells, can bind to HA. This makes HA a good marker for targeted drug delivery for cancer cells [43].

2.4.4 Aptamers

Aptamers are stable and high-affinity ligands used instead of antibodies for targeted drug delivery [44]. Aptamers are short DNA or RNA oligonucleotides consisting of 15-40 bases of 5-15 kDa total molecular weight, also called synthetic antibodies. They are selected by systematic evolution of ligands by exponential enrichment (SELEX). If the sequence is set as an aptamer, there can be easy re-synthesizing. Aptamers are small, have no immunogenicity, are non-toxic and can distinguish between healthy and cancer cells. Aptamers can recover their activity even after denaturation by temperature. Aptamers have a high binding affinity and high specificity by folding into complex 3-dimensional structures. A disadvantage of the use of aptamers is that they have rapid blood clearance because of nuclease degradation [8, 43].

2.4.5 VHH

The variable heavy chain domain of a heavy-chain-only antibody (VHH), also called nanobodies, are great biological ligands due to their characteristics. Firstly, they are conformational and thermally stable. They keep the antigen binding specificity for a week at body temperature, which improves the shelf-life of VHHs compared to immunoglobulins. VHHs also have reversible folding, they keep their antigen binding affinity when incubated at 90°C for long times, where antibodies undergo denaturation and lose their affinity. Next to the thermal stability, VHHs can resist extreme pH and cleavage by proteases [48]. VHHs also have low immunogenicity, which results in the possibility of prolonged and repeated administrations [49]. The CDR1-CDR3 region is the antigen binding region, and the CD3 region on the VHH is longer than that of regular antibodies. This can lead to better recognition of hidden or buried epitopes of tumors for example [48].

VHHs originate from peripheral blood cells of immunized camelids. They are single-chain VHH antibody fragments and have a small size ($\sim$4 by $\sim$2.5 nm) of $\sim$15kDa, which can be seen in figure 2.2 [50]. They are cloned in such a way that they have a high affinity and specificity for the target, so they have easy selection. They have a small size, which leads to rapid extravasation of the VHHs and fast diffusion into the target area [49]. However, the small size could lead to filtration by the kidney (<60kDa) [48]. The rapid extravasation is not beneficial for tumor treatment, where longer accumulation time will result in longer time between

injections, and allows lower doses but still with a high loading yield to the target. By binding to albumin, the blood retention time gets prolonged [49].

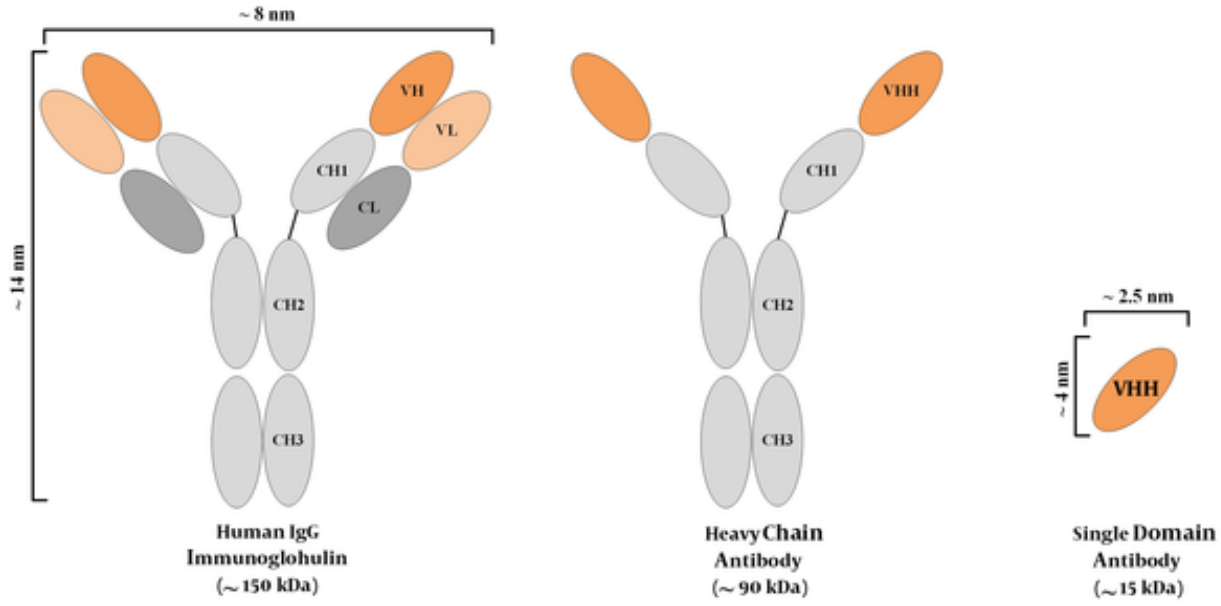

Figure 2.2: Schematic representation of an antibody, the heavy chain antibody and a VHH [50].

2.5 Conjugation techniques

The coupling of the biological ligand to the drug carrier (NPs) can happen through various conjugation techniques. The coupling is important for the system to perform a controlled release of the drug at a specific site [51]. Conjugation techniques can be divided into two types, covalent and non-covalent binding methods. Non-covalent interactions are mostly weaker bindings. The main advantage of non-covalent bindings is that they are reversible. This makes it possible to create an adaptable drug delivery system for certain physiological conditions. For example, a certain environment inside the human body [52]. Covalent binding leads to high yield, mild reaction conditions, easy control and easy removal of side products. It results in stable products that are irreversible, compared to non-covalent binding [53].

The following sections explain the different classes of conjugation techniques, which are electrostatic and hydrophobic interactions, host-guest interactions and click-chemistry. A linker between the biological ligand and the NP can be added, for example, peptide or Polyethylene glycol linkers [54].

2.5.1 Electrostatic and hydrophobic interactions

Electrostatic and hydrophobic interactions form non-covalent bindings. Electrostatics are the interactions between charged molecules, which can be attractive or repulsive forces. Molecules with the same charge (negative or positive) are repulsive of each other. Cationic (positive) molecules are attracted to anionic (negative) molecules. The binding gets strong with a larger charge difference between the two molecules [55].

Hydrophobic interactions are a phenomenon in which non-polar (hydrophobic) molecules aggregate in an aqueous environment. Since water molecules favor forming hydrogen bonds with each other rather than interacting with hydrophobic molecules. This leads to the hydrophobic molecules being excluded from the water, which leads to aggregation. Hydrophobic interactions are possible between hydrophobic nanoparticles and hydrophobic biological ligands, they will form an interaction between the hydrophobic regions. It is a stable interaction because the aggregation minimizes their exposure to water [56].

2.5.2 Host-Guest interactions

Host-guest interactions form complexes by using non-covalent bindings and structural relations between two molecules. This type of conjugation is commonly used in the human body, such as enzyme-inhibitors interaction and antigen-antibody interactions [53]. An example of host-guest interaction is the binding between biotin-streptavidin. The nanoparticle needs to be coated in streptavidin and the ligand or target in biotin. In nature, this is one of the strongest non-covalent conjugation interactions. They have a high affinity for each other and a high specificity, which makes these interactions very stable. However, a disadvantage is that the separation of the biotin from streptavidin can happen under tough conditions, for example a low pH or high-temperature [57].

2.5.3 Click-chemistry

Click-chemistry has been widely utilized for the conjugation of biological ligands, this facilitates the control of the location of the modification on the nanoparticles. For the click-chemistry, various chemical strategies can be used. These strategies have selective coupling of two functional groups that are non-natural and inert to other functional groups. These reactions have covalent bindings and result in a strong and stable product in the biological environment [14]. Click-chemistry results in high yield, strong bindings and simple reaction conditions [58]. A few examples of click-chemistry are maleimide-thiol, azide-alkyne and strain-promoted-azide-alkyne-click reactions, which are explained in the next sections.

Maleimide-thiol

Maleimide-thiol reactions are Michael addition reactions and are commonly applied to biofunctionalize nanoparticles, due to their high reactivity with mild conditions [59]. This type of reaction has several advantages, the reaction can use multiple different functional thiols that are commercially available, spatial control of the chemical modification is possible and it is an orthogonal ligation reaction [58]. The reactions can happen between a maleimide with an unsaturated carbonyl on the NP and a thiol group located on the biological ligand, which results in a stable thioether bond. For example, peptides have free thiol groups in their cysteine residues that can react with the maleimide on the NP [58]. The reaction does not require an initiator and proceeds at room temperature at a neutral pH. However, conditions with a pH8 can result in ring opening, forming a maleic acid amide derivative that is not reactive to thiol groups [59]. Selective maleimide-thiol reactions can be initiated by temperature or UV radiation.

Azide-alkyne cycloadditions (AAC)

Azide-alkyne cycloadditions are reactions that result in stable triazole bonds. A catalyst can be used to accelerate the reaction and improve the yield. Different metals can be used as catalysts, the most common of which are copper and ruthenium. The use of metals can be avoided by activating the alkyne. Copper-catalyzed reactions have the coupling of an azide with a linear alkyne, a regiospecific 1,4-disubstitution is done [60]. It is an insensitive and orthogonal ligation reaction, with a high efficiency [61].

Strain promoted Azide-alkyne click reaction (SPAAC)

SPAAC is another type of azide-alkyne cycloaddition, but without using catalyst like metals that are cytotoxic to cells in the human body. Dibenzocyclooctyne (DBCO) can be used as alkyne and react with an azide via a click-chemistry reaction. It is an orthogonal reaction resulting in a high yield [62]. A catalyst is not needed, due to a decreased activation energy compared to AACs [63]. The NP with the DBCO group reacts with the azide group on the biological ligand. This results in a strong triazole binding [62].

According to L.E. Swart et al. Click chemistry is favorable over Michael additions for direct-surface conjugation, because of better controllability of the coupling reaction and the specific positioning of reactive groups [12].

2.6 Techniques for LNP characterization and conjugation efficiency

To make the targeted drug delivery as effective as possible, the properties of the NPs need to be optimized. These characteristics can be measured using various techniques. Important parameters to measure in order to characterize the NPs are shape, size and surface charge. Dynamic light scattering (DLS), zeta-potential and scanning light microscopy (SEM) can measure these particle properties [64]. SDS-page and Western blot can be used to investigate the conjugation efficiency of the NPs with the biological ligands. These techniques can identify and quantify proteins.

2.6.1 Dynamic light scattering (DLS)

Dynamic light scattering is a common technique used for NPs to measure the size of the NPs and the size distribution. The distribution provides knowledge about the aggregation of the NPs. DLS measures the hydrodynamic size of the NPs in suspension. It also measures the polydispersity index (PDI) of the sample [64]. A PDI of 0 means a monodisperse sample, and a PDI of 1 means polydisperse NPs. Particles with a PDI below 0.3 are acceptable for liposomal NPs [65]. DLS measures the size of the particles by detecting the Brownian motion of the NPs. The Brownian movements of the particles cause constructive and destructive interference, the changes in intensity are time-dependent and measured by DLS. The scattered light is coupled to a specific particle diameter and the size distribution is derived. However, DLS also has some disadvantages. Firstly, with DLS it is difficult to quantify the amounts of aggregates accurately. Secondly, DLS assumes the NPs are spherical. This can lead to an underestimation of the NP size. Lastly, heterogeneous size samples are difficult to interpret the data from [66].

Zeta-potential

Zeta-potential measurements provide knowledge about the surface charge of the NPs. This parameter is important for how stable the particles are. The stability of a particle depends on van der Waals forces and electrical repulsion forces [24]. NPs with a charge of $\pm$10 mV are considered neutral, a charge of +30 mV is strongly cationic and -30mV results in strong anionic particles [26].

The zeta-potential can be measured using a Zetasizer/DLS. It is a non-invasive technique that requires minimal sample preparation. It measures the repulsion or attraction forces between the different particles. An electric field is applied, and the particles move towards or away from the electrodes. The particles scatter the light of a laser at different frequencies. The frequency shift compared to the incident laser frequency is proportional to the speed of the particles, also referred to as the Doppler shift. The velocity obtained from the Doppler shift is calculated to the zeta-potential via multiple mathematical equations [67].

2.6.2 Scanning electron microscope (SEM)

Scanning electron microscopy (SEM) can be used to obtain information about the size and shape of the NPs. It provides topographical information about the NPs and creates secondary electron images using electrons instead of light. An electron gun emits a beam of electrons, the beam is focused on the sample via multiple electromagnetic lenses and a vacuum. Electrons and X-rays are ejected from the sample and collected at the detector, which converts them into a signal, which can be seen as the image. SEM has a very high resolution and a large depth of field. This allows to look into much bigger magnifications of the sample than traditional light microscopes [68].

2.6.3 SDS-page

Sodium dodecyl-sulfate polyacrylamide gel electrophoreses (SDS-page) can be used to test the conjugation efficiency. By using this technique, it can be determined if the conjugation of the NP to the biological ligand happened correctly. SDS-page separates proteins based on molecular mass. Firstly, the proteins are denaturated and coupled to an anionic detergent proportional to their molecular mass. After denaturation,

the proteins are transferred to a porous acrylamide gel. An electric field is applied and the proteins are separated by electrophoresis, based on their molecular mass. After electrophoresis, the protein fragments can be compared to a known protein ladder, to estimate the size of the protein fragments. However, SDS-page is limited due to denaturation of the proteins in advance of the electrophoresis. This means that protein binding interactions and enzyme activity cannot be measured [69].

2.6.4 Western-blot

Western blot can be used to detect, identify and quantify proteins in a complex mixture. It can be used to research the conjugation efficiency of the targeted drug delivery system. First, the proteins are separated based on molecular weight by gel electrophoresis, SDS-page is commonly used. Then the proteins are transferred onto a protein-binding membrane using an electric field. The membrane is incubated with labeled antibodies to specific proteins of interest. After incubation, the bounded antibodies can be detected. A fluorescent label can be used and visualize the bands using a fluorescence imaging system. The proteins can be quantified using the thickness of the bands [70, 71].

Chapter 3

Materials and methods

This chapter discusses the materials and methods used for the experiments. Firstly, the materials with their manufacturers are discussed. Followed by a detailed description of the methods used. Lastly, how the analysis for the results will be performed.

3.1 Materials

The DSPE-PEG(5000)-Mal and DSPE-PEG(2000)-Mal were ordered from BLD Pharmatech GmbH. Cy3-PEG2000-SH (Cy3 dye) was ordered from Biopharma PEG Scientific Inc. The DSPE-PEG(2000)-DBCO and DSPE-PEG(5000)-DBCO were ordered from BroadPharm. The 4arm-Mal-20k and 8arm-Mal-40k, used as control, were ordered from JenKem Technology. MilliQ-water was used from Milli-Q Advantage A10 system (Merck KGaA, Darmstadt, Germany) equipped with a 0.22 μm Millipak®-40 Express filter. The 3.5 and 6-8 and 50 MWCO Spectra/Por® 6 dialysis membranes were ordered from Spectrum Laboratories. The 96 wells-plates used for fluorescence measurements are Microfluor Black flat bottom plates from Greiner. For SDS-page, Mini-Protean-TGX-Precast Gels 4-15% were used and ordered from Bio-Rad Laboratories. The β-Mercaptoethanol and laemmli for the buffer solution and the Precision PlusProtein WesternC Protein ladder were also ordered from Bio-Rad Laboratories.

The following materials were ordered from Sigma Aldrich: L-Cysteine hydrochloride, used for blocking the samples with maleimide. Azido-PEG3-amine, used for blocking the samples with DBCO. Tris (2-carboxyethyl) phosphine hydrochloride solution (TCEP) 0.5M, used as reducing agent. The 10 MWCO Amicon Ultra and Vivaspin 30 MWCO spinfilters and PBS.

The LNPs used for the experiments were prepared at the University of Utrecht with a NanoAssemblr™. Except the LNPs used for post-insertion with DSPE-PEG-Mal-VHH, these were made at the UT, using a Herringbone microfluidic mixer, with mCherry as mRNA. The VHHs were obtained from Orthros Medical.

3.2 Methods

This section discusses the methods used for the experiments. Firstly, the method for the synthesis of the LNPs will be discussed. Secondly, the conjugation of DSPE-PEG-Mal/DBCO to Cy3-PEG-SH/Azide-PEG-Cy3 dye will be discussed followed by the post-insertion of the DSPE-PEG-Mal/DBCO-Cy3. Lastly, the conjugation of the DSPE-PEG-Mal to VHHs will be discussed followed by the post-insertion of the DSPE-PEG-Mal-VHH.

3.2.1 LNPs fabrication

First, the lipid stock solution and the mRNA stock solution were made. The lipid stock solution consists of Dlin-MC3-DMA (20 mg/ml), DSPC (10 mg/ml), cholesterol (10 mg/ml), DMG-PEG2000 (10 mg/ml) and PEG-lipid-Cy5.5 (1 mg/ml) in a molar ratio of 50:10:38.3:1.4:0.2 %, with ethanol as solvent. The mRNA

stock solution contained 100 μg mRNA added to 1050 μl with Sodium acetate buffer (100 mM, pH4) solution. The LNPs were made with the help of a microfluidic chip with a herringbone structure. The lipid stock solution had a flow of 250 μL/min and the mRNA stock solution had a flow of 750 μL/min. The LNPs were dialyzed against Milli-Q water for at least 1 hour using 50 MWCO membranes and stored in the fridge at 4 °C.

3.2.2 Synthesis of an Azide functional Cy3 dye

For the conjugation of the Azide to Cy3-PEG2000-SH, first TCEP was used as reducing agent for the dithiol bonds between the Cy3-PEG2000-SH molecules. A threefold molar excess of TCEP is added to Cy3-PEG2000-SH and left to react in 0.5 ml DMSO for 1 hour at 37 °C. At the same time, Azido-PEG3-amine is left to react with Maleimide-NHS-ester (N-α-maleimidoacet-oxysuccinimide ester) in a molar ratio of 3:2 at room temperature for 30 minutes. After both reactions have occurred, the mixtures are added in a molar ratio of 1:10:15(Cy3-PEG2000-SH:Maleimide-NHS-ester:azido-amine) and left to react overnight at 37 °C while stirring. The DMSO was removed under vacuum and the product was dissolved in PBS, dialyzed overnight in Float-A-Lyser with a MWCO of 500-1000 Da and finally freeze-dried to obtain the Azide-PEG2000-Cy3 dye. The reaction with structure formulas of the components can be seen in figure 3.1.

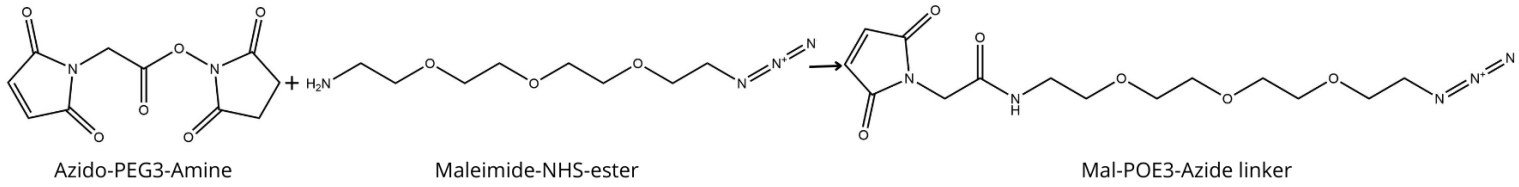

(a)

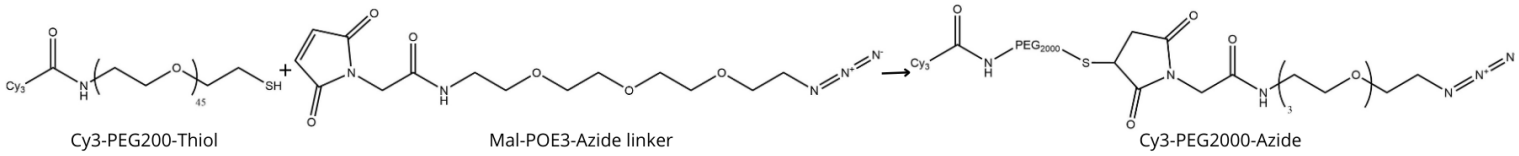

(b)

Figure 3.1: The chemical reaction of the synthesis of Azide-PEG2000-Cy3,with corresponding structure formulas of the components. (a) Step 1 of the reaction, Azido-PEG3-Amine reacting with Maleimide-NHS-ester to form Mal-PEO3-Azide linker. (b) Step 2 of the reactoin, Cy3-PEG2000-Thiol reacting with Mal-POE3-Azide linker to form Cy3-PEG2000-Azide.

3.2.3 Conjugation of lipids to Cy3 dyes

The conjugation of DSPE-PEG-Mal/DBCO to the Cy3 dye will be discussed in this section. The two reactive groups were tested: DSPE-PEG-Mal and DSPE-PEG-DBCO. The DSPE-PEG-Mal were coupled to Cy3-PEG2000-SH and the DSPE-PEG-DBCO were coupled to Azide-PEG2000-Cy3.

DSPE-PEG-Mal to SH-PEG2000-Cy3

The coupling of DSPE-PEG-Mal to Cy3-PEG2000-SH was performed with lipids containing PEG spacers of 2000 and 5000 Da, the reaction can be seen in figure 3.2. DSPE-PEG2k-Mal had a concentration of 0.25 mg/ml in PBS and DSPE-PEG5k-Mal had a concentration of 0.5 mg/ml in PBS. The Cy3-PEG2000-SH dye was treated with TCEP as reducing agent for the dithiol bonds between Cy3-PEG2000-SH molecules. A molar ratio of 1:10 (Cy3-PEG2000-SH:TCEP) reacted for 1 hour at 37 °C. After the dye was reduced with TCEP, an excess of Cy3-PEG2000-SH was added to the DSPE-PEG-Mal in a 1:3 (DSPE-PEG-Mal:Cy3-PEG2000-SH) ratio. All samples were vortexed, centrifuged and left to react overnight at 4 °C. After incu-

bation, dialysis was used to remove the non-reacted Cy3-PEG2000-SH. All samples were dialyzed against Milli-Q water overnight. Reaction mixtures with DSPE-PEG-Mal containing PEG spacer of 2 kDa and 5 kDa were dialyzed with 3.5 kDa and 6-8 kDa MWCO membranes. After dialysis, all samples were freeze-dried with the Lyovapor L-200 from BÜCHI Labortechnik GmbH. As control, DSPE-PEG(2000 and 5000)-Mal were blocked with L-Cysteine hydrochloride. A molar ratio of 1:10 (DSPE-PEG-Mal:Cysteine) reacted for 1 hour at room temperature. Afterward, conjugation was performed as described above.

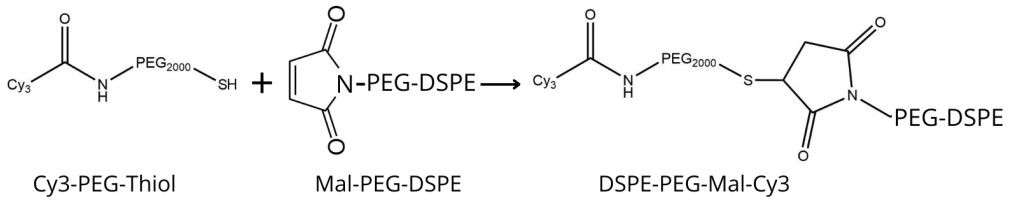

Figure 3.2: The chemical reaction of the synthesis of DSPE-PEG-Mal-Cy3, Cy3-PEG-Thiol reacting with Mal-PEG-DSPE, with corresponding structure formulas of the components.

DSPE-PEG-DBCO to Azide-PEG2000-Cy3

The coupling of DSPE-PEG-DBCO to the Azide-PEG2000-Cy3 was performed with DSPE-PEG-DBCO containing PEG spacers of 2000 and 5000 Da, the reaction can be seen in figure 3.4 DSPE-PEG-DBCO had a concentration of 0.25 mg/ml (2 kDa PEG) and 0.5 mg/ml (5 kDa PEG) dissolved in PBS. Azide-PEG2000-Cy3 was added in excess to DSPE-PEG-DBCO in a 1:3 (DSPE-PEG-DBCO:Azide-PEG2000-Cy3) molar ratio. All samples were vortexed, centrifuged and left to react overnight at 4 °C. After incubation, dialysis was used to remove the non-reacted Azide-PEG2000-Cy3. Reaction mixtures with DSPE-PEG-DBCO containing a PEG spacer of 2 kDa and 5 kDa were dialyzed with 3.5 kDa and 6-8 kDa MWCO membranes respectively. After dialysis, all samples were freeze-dried with the Lyovapor L-200 from BÜCHI labortechnik GmbH. As positive control, 4-arm-PEG-Mal was used. As negative control, 4-arm-PEG-Mal was blocked with a 10-fold L-Cysteine hydrochloride and reacted for 1 hour at room temperature. Afterward, conjugation was performed as described above.

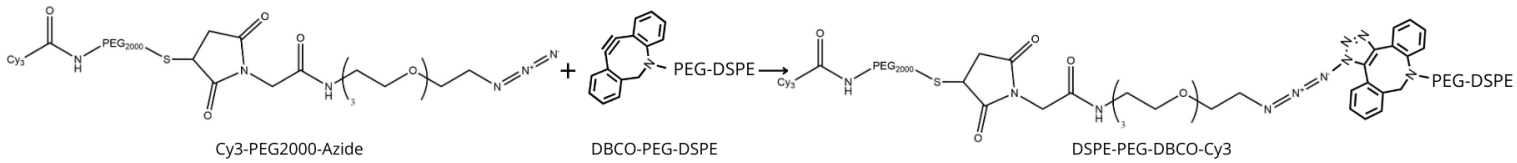

Figure 3.3: The chemical reaction of the synthesis of DSPE-PEG-DBCO-Cy3, Azide-PEG2000-Cy3 reacting with DBCO-PEG-DSPE, with corresponding structure formulas of the components.

3.2.4 Conjugation of lipids to VHHs

The conjugation of the lipids to the VHHs will be discussed in this section. Only one reactive group was tested, DSPE-PEG-Mal with a PEG spacer of 5000 Da.

DSPE-PEG-Mal to VHH

The coupling of DSPE-PEG-Mal to VHH was performed with DSPE-PEG-Mal containing PEG spacers of 5000 Da. DSPE-PEG-Mal had a concentration of 0.20 mg/ml in PBS. VHHs were added in a molar ratio of 5:1 (DSPE-PEG-Mal:VHH). All samples were vortexed and centrifuged and left to react overnight at 4 °C. After incubation, spinfiltration was used to remove the non-reacted DSPE-PEG-Mal. All samples were

spinfiltered four times at 14000g for 30 minutes with 10 kDa MWCO spinfilters, with PBS as washing agent. As positive control, 8-arm-PEG-Mal was used in a molar ratio of 5:1 (8-arm-PEG-Mal:VHH). As negative control, DSPE-PEG5k-Mal was blocked with a 100-fold L-Cysteine hydrochloride and reacted for 1 hour at 37 °C. Afterwards, conjugation was performed as described above.

For the repeated conjugation reaction. The VHHs were treated with TCEP as reducing agent for the dithiol bonds between VHH molecules. A molar ratio of 1:3 (VHH:TCEP) reacted for 1 hour at 37 °C. Afterwards, conjugation was performed as described above.

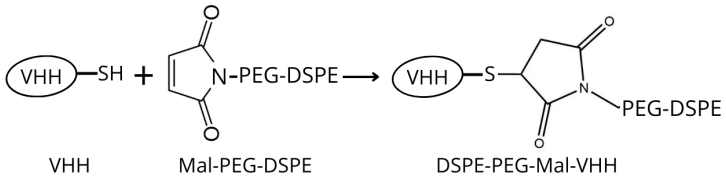

Figure 3.4: The chemical reaction of the synthesis of DSPE-PEG-Mal-VHH, VHH-Thiol reacting with Mal-PEG-DSPE, with corresponding structure formulas of the components.

3.2.5 Post-insertion

The post-insertion was done after dialysis of the LNPs (see section 3.2.1 for the composition). The following lipids were post-inserted into the LNPs: DSPE-PEG2000-mal-Cy3, DSPE-PEG5000-mal-Cy3, DSPE-PEG2000-DBCO-Cy3, DSPE-PEG5000-DBCO-Cy3 and DSPE-PEG5000-Mal-VHH. Molar ratios of 0.1%, 0.2% and 0.3% of the lipids were tested. The concentration of DSPE-PEG-DBCO/Mal-Cy3 and LNPs were determined using the calibration curves of Cy3 and Cy5.5 dyes respectively, see section 3.3.2. The concentration of DSPE-PEG-Mal-VHH was determined using absorbance measurements with the Nanodrop. A rough estimate of the concentration is made by measuring the absorbance at a wavelength of 280 nm and calculating the concentration based on this absorbance. The assumption is made that 1 absorbance unit is equal to a concentration of 1 mg/ml. With the concentrations and the molarities, the number of lipids was calculated.

DSPE-PEG-Mal-Cy3

The post-insertion of DSPE-PEG-Mal-Cy3 in the LNPs was performed with DSPE-PEG-Mal containing PEG spacers of 2000 and 5000 kDa. The lipid stock solutions of DSPE-PEG(2000 and 5000)-Mal-Cy3 were prepared in molar ratios of 0.1%, 0.2% and 0.3% in PBS. The samples were prepared containing, 100 μl LNPs (0.01 mg/ml), the volume of lipid stock solution needed for every molar ratio and supplemented with PBS to a total volume of 500 μl. All samples were incubated for 30 minutes at 45 °C. After incubation, spinfiltration was used to remove non-inserted DSPE-PEG-Mal-Cy3. All samples were spinfiltered four times at 15000g for 30 minutes in 30 kDa MWCO spinfilters, with PBS as washing agent.

As negative control, Cy3-PEG2000-SH was added to the LNPs in molar ratios of 0.1%, 0.2% and 0.3%. As second control, DSPE-PEG(2000 and 5000)-Mal-Cy3 in a molar ratio of 0.2% was dissolved in PBS. The third control was only LNPs dissolved in PBS. The controls were treated as described above.

DSPE-PEG-DBCO-Cy3

The post-insertion of DSPE-PEG-DBCO-Cy3 in the LNPs was performed with lipids containing PEG spacers of 2000 and 5000 kDa. The lipid stock solutions of DSPE-PEG(2000 and 5000)-DBCO-Cy3 were prepared in molar ratios of 0.1%, 0.2% and 0.3% in PBS. The samples were prepared containing, 100 μl LNPs (0.01 mg/ml), the volume of lipid stock solution needed for every molar ratio and supplemented with PBS to a total volume of 200 μl. All samples were incubated for 30 minutes at 45 °C. After incubation, dialysis was

used to remove non-inserted DSPE-PEG-DBCO-Cy3. All samples were dialyzed overnight against Milli-Q water in 50 kDa MWCO membranes. After purification, all samples were spinfiltered at 14000g for 30 minutes in 3 kDa MWCO spinfilters, to reduce aggregation of the LNPs.

As negative control, Cy3-PEG2000-SH was added to the LNPs in molar ratios of 0.1%, 0.2% and 0.3%. As second control, DSPE-PEG(2000 and 5000)-DBCO-Cy3 in a molar ratio of 0.2% was dissolved in PBS. The third control was only LNPs dissolved in PBS. The controls were treated as described above.

DSPE-PEG5000-Mal-VHH

The post-insertion of DSPE-PEG-Mal-VHH in the LNPs was performed with lipids containing a PEG spacer of 5000 kDa. The lipid stock solutions of DSPE-PEG5000-Mal-Cy3 were prepared in molar ratios of 0.1%, 0.2% and 0.3% in PBS. The samples were prepared containing, 100 μl LNPs (0.01 mg/ml), the volume of lipid stock solution needed for every molar ratio and supplemented with PBS to a total volume of 200 μl. All samples were incubated for 30 minutes at 45 °C. After incubation, spinfiltration was used to remove non-inserted DSPE-PEG-Mal. All samples were spinfiltered four times at 15000g for 30 minutes in 10 kDa MWCO spinfilters, with PBS as washing agent. As control, DSPE-PEG5000-Mal-Cy3 in a molar ratio of 0.2% was dissolved in PBS. The second control was only LNPs dissolved in PBS. The controls were treated as described above.

3.3 Analysis

This section discusses how the results were analyzed. Firstly, the Azide functional Cy3 dye is discussed. Secondly, the conjugated DSPE-PEG-Mal/DBCO-Cy3 followed by the conjugated DSPE-PEG-Mal-VHH. Lastly, the post-insertion of the DSPE-PEg-Mal/DBCO-Cy3 and DSPE-PEG-Mal-VHH will be discussed.

3.3.1 Azide functional Cy3 dye

The product of the conjugation of the Azide-linker to the SH-PEG2000-Cy3 was quantified by measuring the fluorescence with the Varioskan LUX 3020-528 from Thermofisher. The fluorescence of Cy3 (Ex 555 nm, Em 569 nm) was measured in a 96-wells plate, with 100 μl sample in each well. With the help of a calibration curve with known concentrations, an estimate of the concentration of the Azide-PEG2000-Cy3 was determined. To determine if the conjugation occurred, NMR analysis was performed by J. Kossen (Master-student at DBE).

3.3.2 Conjugation lipids-Cy3

The products of the conjugation of the lipids to the Cy3 dyes were quantified by measuring the fluorescence with the Varioskan LUX 3020-528 from Thermofisher. The fluorescence of Cy3 (Ex 555 nm, Em 569 nm) was measured in a 96-wells plate, with 100 μl sample in each well. An estimate of the amount of conjugated lipids was determined using the calibration curve with known concentrations.

3.3.3 Conjugation lipids-VHH

To quantify the conjugation of the lipids to the VHH, an SDS-page was performed. The samples were prepared by mixing 2μg of the sample with 5μl sample buffer (b-mercaptoethanol and Laemmli, 1:9) and the volume was supplemented to 20 μl with PBS. The samples were incubated for 5 minutes at 95 °C. The tank was assembled and the outer lanes of the gel were filled with 5 μl protein ladder, the other lanes were filled with 20 μl sample. The gel was running at 100V for 20 minutes and 160V for 40 minutes under SDS-running buffer. The gel was washed with Milli-Q water for 5 minutes and incubated on a shaker for 30 minutes with fixation solution (50%methanol, 10% acetic acid and 40% H_2O). After fixation, the gel was stained with Coomassie staining solution (fixation solution and 0.25 % w/v Coomassie Blue R-250) for 2–4 hours on a shaker. The gel was destained using a destaining solution (5% methanol, 7.5% acetic acid and 87.5 % H_2O)

for 4–24 hours, the solution was refreshed every 30 minutes for at least the first 2 hours. The gel was imaged with the FluorChem M system from ProteinSample. To quantify the results from the SDS-page, the conjugation efficiency is determined by performing a densitometric analysis with ImageJ. The control lane with only VHH in the sample is set to 100%.

3.3.4 Post-insertion

The post-insertion of DSPE-PEG-Mal/DBCO-Cy3 in the LNPs was quantified by measuring the fluorescence. The fluorescence was measured with the Varioskan LUX 3020-528 from Thermofisher, in a 96-wells plate with 100 μl in each well. The fluorescence of DSPE-PEG-Mal/DBCO-Cy3 was measured for Cy3 (Ex 555 nm, Em 569 nm), and the fluorescence of the LNPs was measured for Cy5.5 (Ex 683 nm, Em 703 nm). The fluorescence of the LNPs post-inserted with DSPE-PEG(2000 and 5000)-DBCO-Cy3 of batch 3 was measured with the Wallac 1420 Victor Platereader. The Cy5.5 fluorescence value can be seen as the amount of LNPs in the sample, assuming every LNP has the same amount of fluorescence. To average out the difference in number of particles, the Cy3 fluorescence was divided by the Cy5.5 fluorescence. The controls without LNPs cannot be divided, since these samples do not contain Cy5.5 fluorescence.

The quantification of the post-insertion with DSPE-PEG-Mal-VHH in the LNPs was performed using SDS-page. Before the SDS-page analysis, the samples underwent purification following the protocol from section 3.3.3. The LNPs fall apart in the SDS-running buffer, allowing for the measurement of the individual lipids on the SDS-page. The assumption was made that all non-inserted lipids were removed during the purification steps.

The hydrodynamic size and the PDI of the post-inserted LNPs with DSPE-PEG-Mal/DBCO-Cy3 and DSPE-PEG-Mal-VHH were obtained by performing DLS measurements with the ZetaSizer Nano Series from Malvern. The LNPs were diluted 1:5 in PBS and transferred into the disposable PMMA cuvettes from VWR. The measurements were performed 3 times at room temperature.

Chapter 4

Results and discussion

This chapter discusses the results of the performed experiments. Firstly, the synthesized LNPs will be analyzed on size and PDI. Secondly, the conjugation of DPSE-PEG-DBCO/Mal to Cy3 dye will be analyzed based on fluorescence measurements. After analyzing the results of DSPE-PEG-DBCO/Mal-Cy3, the results of the post-insertion of DSPE-PEG-DBCO/Mal-Cy3 will be discussed by looking at the fluorescence, size and PDI. After discussing the results of the Cy3 dye conjugation, the conjugation of DSPE-PEG-Mal to VHHs will be analyzed by using SDS-page. After analyzing, post-insertion of DSPE-PEG-Mal-VHH was performed and quantified with an SDS-page and analyzed on size and PDI.

4.1 LNPs fabrication

Table 4.1 shows the results of the DLS measurements performed on the LNPs with mCherry and tRNA. The experiment is performed together with M. Verhoeven (Bachelor student at DBE). The size of the LNPs containing with mCherry have a much smaller size of approximately 100 nm and a smaller standard deviation compared to the LNPs containing tRNA. For the PDI, the same trend is seen. The LNPs containing tRNA are more polydisperse and the LNPs containing mCherry are more monodispersed.

Table 4.1: The hydrodynamic size and PDI of the LNPs made with tRNA and mCherry measured with DLS. Experiment performed together with M. Verhoeven (Bachelor student at DBE).

	Hydrodynamic size (nm)	**Polydispersity Index (PDI)**
LNPs tRNA	212.2 ± 24.3	0.560
LNPs mCherry	122.3 ± 1.0	0.250

4.2 Conjugation DSPE-PEG-DBCO to Azide-PEG2000-Cy3 dye

Figure 4.1 shows the conjugation results from DSPE-PEG-DBCO to Azide-PEG2000-Cy3. This experiment is performed twice together with J. Kossen (master student at DBE), with the batch of Azide-PEG2000-Cy3 and with the same conditions to get sufficient DSPE-PEG-DBCO-Cy3 for the post-insertion experiments. The results of the first batch can be seen in figure 4.1a. DSPE-PEG-DBCO with 2000 PEG shows approximately the same amount of fluorescence as the control with only Azide-PEG2000-Cy3 dye (dialyzed with 3.5 kDa MWCO membrane). This is not as expected, because the Azide-PEG2000-Cy3 should wash out of the membrane since it has a molecular weight under the 3.5 kDa MWCO of the membrane. However, DSPE-PEG-DBCO with 5000 Da PEG shows a higher fluorescence than the control with only Azide-PEG2000-Cy3 dye (dialyzed with 6-8 kDa MWCO membrane), which is as expected. The fluorescence of DSPE-PEG-DBCO with 5000 Da PEG is higher than DSPE-PEG-DBCO with 2000 Da PEG. This indicates that DSPE-PEG-DBCO with 5000 PEG has a higher conjugation to Azide-PEG2000-Cy3 than DSPE-PEG-DBCO with 2000 PEG. The 8-arm-PEG-Mal, negative control, shows a relatively low fluorescence. If the 8-arm-PEG-Mal is blocked, the same amount of fluorescence is measured. This is as expected, since both

8-arm-PEG-Mal and 8-arm-PEG-Mal-blocked should not interact with the Azide-PEG2000-Cy3 dye.

Looking at the second batch in figure 4.1b, DSPE-PEG-DBCO with 2000 Da PEG shows a higher fluorescence than the control with only Azide-PEG2000-Cy3. The same counts for DSPE-PEG-DBCO with 5000 Da PEG. DSPE-PEG-DBCO with 2000 Da PEG shows a lower fluorescence than DSPE-PEG-DBCO with 5000 Da PEG. The 8-arm-PEG-Mal, negative control, shows a low fluorescence. When this molecule is blocked, there is no difference in fluorescence seen compared to the non-blocked 8-arm-PEG-Mal, as expected.

Comparing the two different batches, the second batch has a higher conjugation since the fluorescence values are much higher and the fluorescence of the control samples are all low. DSPE-PEG-DBCO with 5000 Da PEG seems to have a better conjugation efficiency than DSPE-PEG-DBCO with 2000 Da PEG, as shown by the higher fluorescence values. Summarizing, the conjugation between DSPE-PEG-DBCO and Azide-PEG2000-Cy3 took place, but there is the possibility that part of the fluorescence seen is due to non-specific interaction and not conjugation.

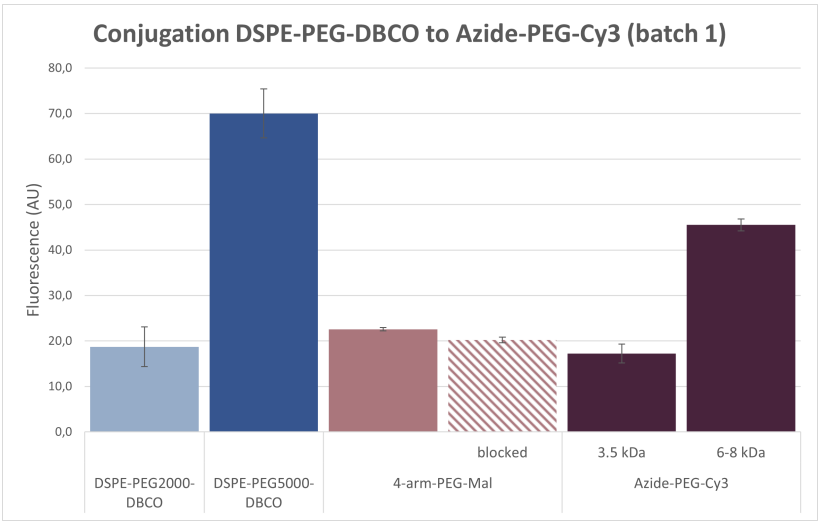

(a)

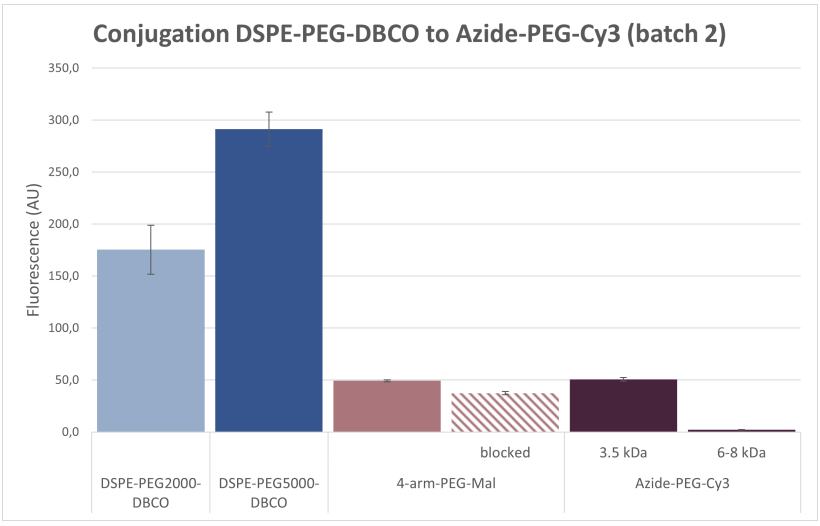

(b)

Figure 4.1: The fluorescence results of the conjugation of DSPE-PEG-DBCO to Azide-PEG2000-Cy3, repeated. The experiment is performed together with J. Kossen (Master-student at DBE). (a) The fluorescence results of the conjugation of DSPE-PEG-DBCO to Azide-PEG2000-Cy3, batch 1. (b) The fluorescence results of the conjugation of DSPE-PEG-DBCO to Azide-PEG2000-Cy3, batch 2.

4.3 Conjugation DSPE-PEG-Mal to Cy3-PEG-SH dye

In figure 4.2 the results from the coupling of DSPE-PEG-Mal to Cy3 can be seen. This is a repeated experiment, resulting in batch 1 and batch 2. The fluorescence of batch 1 can be seen in figure 4.2a. The fluorescence for DSPE-PEG-Mal with 2000 Da and 5000 Da PEG are both higher than the blocked control samples.
DSPE-PEG-Mal with 5000 Da PEG shows a higher fluorescence signal than DSPE-PEG-Mal with 2000 Da PEG, this implies that more DSPE-PEG-Mal with 5000 Da PEG is conjugated to Cy3-PEG-SH. The control with only Cy3-PEG-SH dye shows for DSPE-PEG-Mal with 2000 Da PEG (dialyzed in 3.5 kDa MWCO membrane) a similar fluorescence as blocked DSPE-PEG-Mal with 2000 Da PEG. However, the control sample with only Cy3-PEG-SH dye for DSPE-PEG-Mal with 5000 Da PEG (dialyzed in 6-8 kDa MWCO membrane) has a lower fluorescence than blocked DSPE-PEG-Mal with 5000 Da PEG. Overall, this indicates the blocking of the maleimide is not working properly or DSPE-PEG-Mal interacts with Cy3-PEG-SH by hydrophobic non-specific interactions. A second dialysis of batch 1 is performed, the results can be seen in figure 4.2b. The fluorescence of the non-blocked samples stays the same for DSPE-PEG-Mal with 2000 Da and 5000 Da PEG and is higher than the blocked samples, so conjugation did occur. The fluorescence of only Cy3-PEG-SH decreases for both MWCO membranes, which means the unconjugated Cy3-PEG-SH dye filters out of the membranes. However, the blocked samples retain the same fluorescence. This could be because the blocking did not work properly so DSPE-PEG-Mal is conjugated to Cy3-PEG-SH or there is a lot of hydrophobic non-specific interaction with DSPE-PEG-Mal to Cy3-PEG-SH. Both make the molecules too big to be dialyzed out of the 3.5 or 6-8 kDa MWCO membranes.

Batch 2 is dialyzed once, the results can be seen in figure 4.2c. The same trends can be seen for batch 2 as in batch 1. The fluorescence is higher for DSPE-PEG-Mal with 2000 Da and 5000 Da PEG than the blocked control samples. In this batch, the fluorescence is higher for DSPE-PEG-Mal with 2000 Da PEG than DSPE-PEG-Mal with 5000 Da PEG. The control with only Cy3-PEG-SH dye is for the 3.5 kDa MWCO membrane (2000 Da PEG) the same as the blocked DSPE-PEG-Mal with 2000 Da PEG control. For the 6-8 kDa MWCO membrane the fluorescence signal of the dye control is almost zero, while the blocked DSPE-PEG-Mal with 5000 Da PEG shows a significant fluorescent signal, confirming the first experiment.

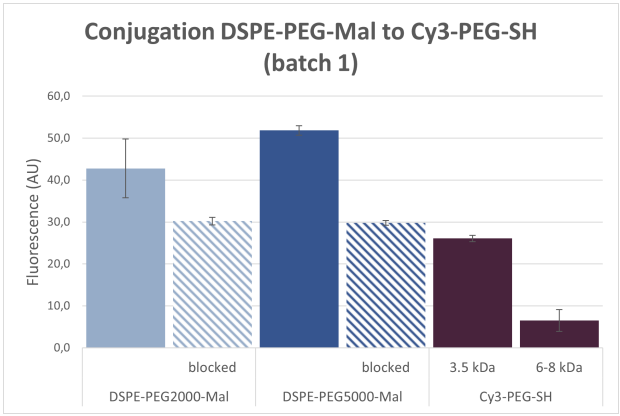

(a)

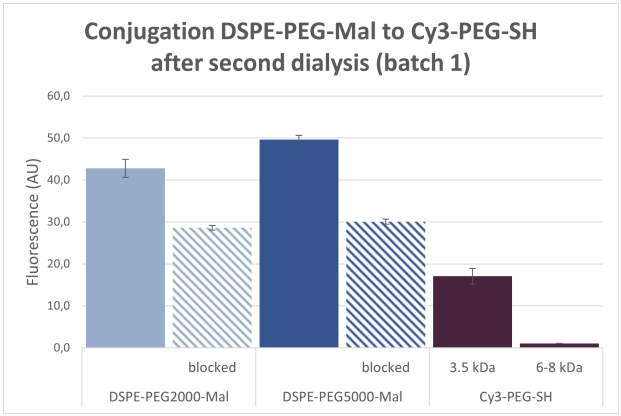

(b)

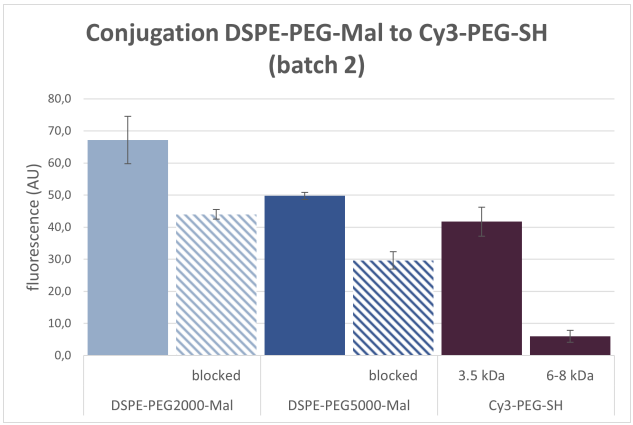

(c)

Figure 4.2: The fluorescence results of the conjugation of DSPE-PEG-Mal to Cy3-PEG-SH. (a) The fluorescence results of batch 1 after the first dialysis. (b) The fluorescence results of batch 1 after the second dialysis. (c) The fluorescence results of batch 2 after the first dialysis.

Summarizing, both batches show conjugation. However, there could still be a lot of hydrophobic non-specific interactions, based on the results of the blocked maleimide control samples. Further experiments should be performed to discriminate between conjugation and non-specific interaction. in batch 1 shows DSPE-PEG-Mal with 5000 Da PEG a better conjugation than DSPE-PEG-Mal with 2000 Da PEG, seen in the higher amount of fluorescence. This is not seen in batch 2.

For future experiments of the conjugation of DSPE-PEG-Mal and DSPE-PEG-DBCO to Cy3-PEG-SH and Azide-PEG2000-Cy3, it can be tested if the blocking is not working properly or if there is non-specific interaction. To test if the blocking is causing the high fluorescence, another blocking molecule can be used. For example dithiothreitol (DTT) for blocking Maleimide reactive groups and 3-Azido-1-propanol to block DBCO reactive groups [72, 73]. There can also be tested if the cysteine, used for blocking, is forming disulfide bonds between molecules, by treating the cysteine with a reducing agent like TCEP. To examine if hydrophobic non-specific interactions take place, a hydrophilic dye can be used. In this way, the hydrophilic dye should not interact with the hydrophobic DSPE-PEG-Mal/DBCO and result in no conjugation. For example FITC-PEG-SH dye could be used [74]. This has no overlap in the excitation and emission wavelength of the Cy5.5 dye and is hydrophilic. Another option to examine the hydrophobic non-specific interaction is to take another control into account, namely lipids without Mal or DBCO as reactive group. Because the Cy3 dye should interact with the lipids if it would be hydrophobic non-specific interactions.

For the post-insertion of DSPE-PEG-Mal/DCBO-Cy3, the assumption is made that all the unconjugated Cy3 dye is dialyzed out of the membranes during the synthesis of DSPE-PEG-Mal/DBCO-Cy3. However, the dialysis membranes turned pink during the purification because of the Cy3 dye. This means that the

Cy3 dye could have blocked the pores and the dialysis membranes could not filter out all the unconjugated Cy3 dye molecules. This phenomenon has been seen more in the 3.5 kDa MWCO membranes than in the 6-8 kDa MWCO membranes. This explains why there is still fluorescence seen in the samples with only Azide-PEG2000-Cy3 and Cy3-PEG-SH dye in figure 4.1 and 4.2.

4.4 Post-insertion DSPE-PEG-DBCO/Mal-Cy3

The post-insertion performed with DSPE-PEG-Mal-Cy3 was inconclusive and can be seen in appendix A1. The same applies for the post-insertion with DSPE-PEG-DBCO-Cy3 for batch 1, these results can be seen in appendix A2. The protocol of this experiment was optimized and performed another two times with DSPE-PEG-DBCO-Cy3 into LNPs. Three different molar ratios of DSPE-PEG-DBCO-Cy3 are tested: 0.1, 0.2 and 0.3 %. Three controls are taken into consideration. A sample without LNPs, without DSPE-PEG-DBCO-Cy3 and lastly a sample with only Cy3-PEG-SH and LNPs.

4.4.1 Post-insertion DSPE-PEG-DBCO-Cy3 Batch 2

Figure 4.3 shows the fluorescence results of the second post-insertion with DSPE-PEG-DBCO-Cy3. In figure 4.3a, the Cy3 fluorescence of DSPE-PEG-DBCO-Cy3 can be seen. There is an increase in fluorescence with an increase in molar ratio of DSPE-PEG-DBCO-Cy3. The DSPE-PEG-DBCO-Cy3 with 5000 Da PEG shows a higher fluorescence than the DSPE-PEG-DBCO-Cy3 with 2000 Da PEG. The control with only Cy3-PEG-SH added shows almost no fluorescence, as expected since the unconjugated Cy3-PEG-SH should dialyze out of the membranes. The control with only LNPs shows no Cy3 fluorescence, as expected since there is no DSPE-PEG-DBCO-Cy3 present. However, the two control groups with only DSPE-PEG-DBCO-Cy3 with 2000 and 5000 Da PEG 0.2% and no LNPs show relatively high fluorescence. This could imply that DSPE-PEG-DBCO/Cy3 is not dialyzed out of the membranes. The Cy5.5 fluorescence can be seen in figure 4.3b, this is the fluorescence of the LNPs. The fluorescence fluctuates for every sample, but it has less fluctuation than the first batch in figure A.3b. The control with only DSPE-PEG-DBCO-Cy3 shows no fluorescence, as expected since there are no LNPs added in the sample.

To average out the difference in the number of particles the Cy3 fluorescence is divided by the Cy5.5 fluorescence. The Cy3/Cy5.5 values can be seen in figure 4.3c. There is an increase in fluorescence with an increase in molar ratio for the post-inserted DSPE-PEG-DBCO-Cy3. The post-inserted DSPE-PEG-DBCO-Cy3 with 5000 Da PEG shows a higher fluorescence than DSPE-PEG-DBCO-Cy3 with 2000 Da PEG. The control group with only Cy3-PEG-SH shows low fluorescence values, there is an increase in fluorescence with an increase of molar ratio of the Cy3-PEG-SH. The LNPs as control show a value of 0 fluorescence, as expected.

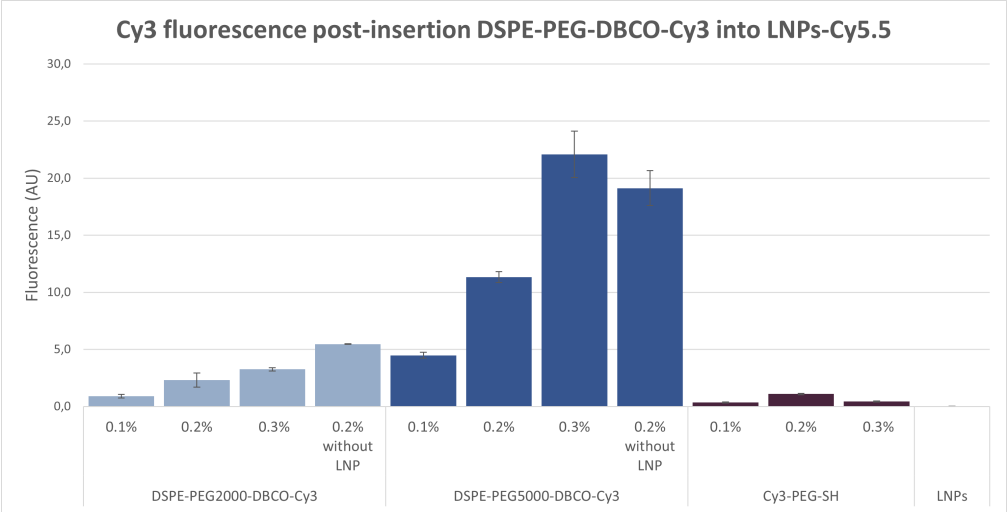

(a)

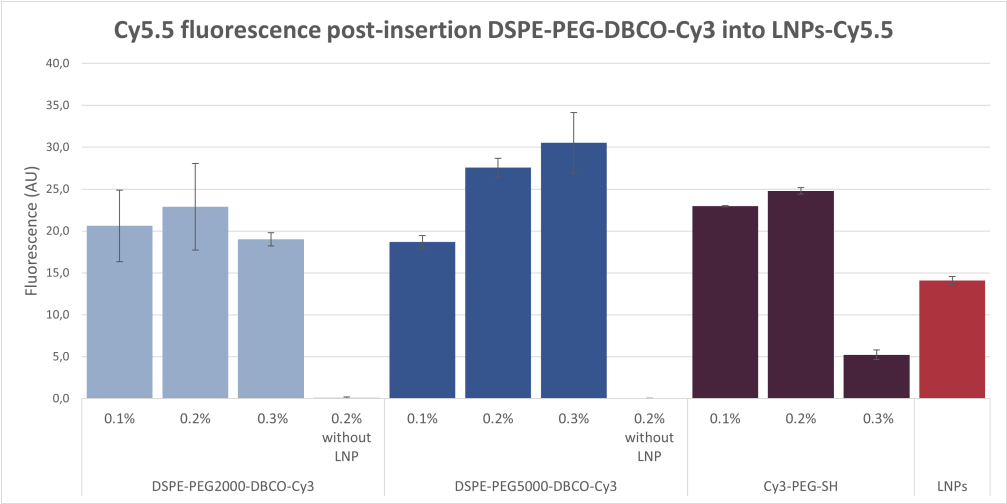

(b)

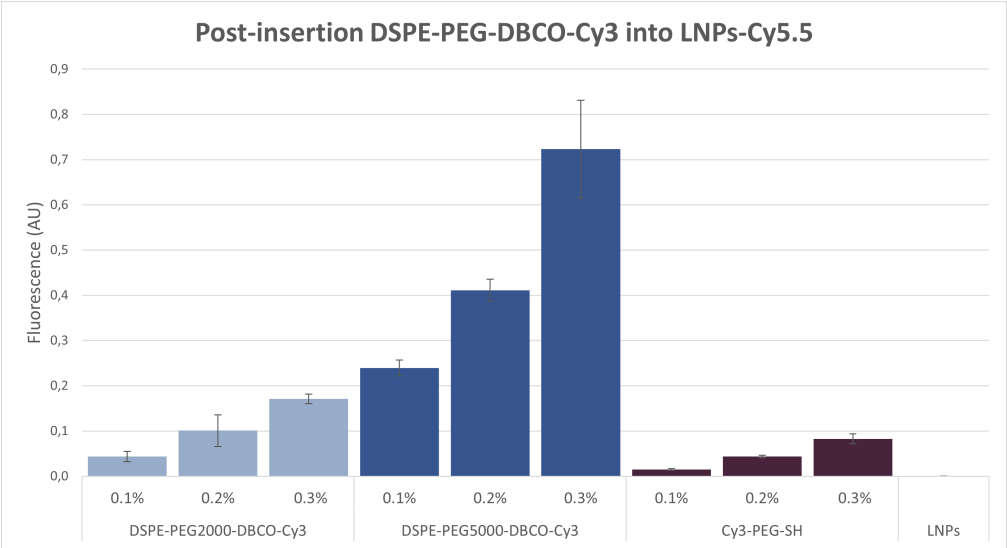

(c)

Figure 4.3: The fluorescence results of the post-insertion with DSPE-PEG-DBCO-Cy3 into the LNPs of batch 2. (a) The Cy3 fluorescence of DSPE-PEG-DBCO-Cy3. (b) The Cy5.5 fluorescence of the LNPs, sample with Cy3 dye 0.3% has fewer LNPs added. (c) Averaged out values are Cy3 values divided by Cy5.5 values to average out the difference in the number of particles present in each sample.

The DLS data of the post-insertion with DSPE-PEG-DBCO-Cy3 is shown in table 4.2. The PDI of these samples cannot be shown, since there was aggregate formation, but the standard deviation of the LNP sizes indicates the polydispersity of the sample. The same results are visualized in a graph, which can be seen in figure 4.2. The DLS data shows that the size decreases if the LNPs are spinfiltered, for the LNPs and as well for the LNPs post-inserted with DSPE-PEG-BDCO-Cy3 with 2000 Da PEG 0.1 %. The post-insertion of DSPE-PEG-DBCO-Cy3 with 2000 Da PEG 0.1 and 0.2 % leads to an increase in size of approximately 100 nm. The size of the LNPs does not increase significantly for the post-insertion with DSPE-PEG-DBCO-Cy3 with 5000 Da PEG 0.3 %. The size of the control samples with only Cy3-PEG-SH present does not increase significantly. However, there are particles measured in the samples without LNPs, this is not as expected since there are no LNPs present in this sample. For the DSPE-PEG-DBCO-Cy3 with 2000 Da PEG, this is a size of approximately 900 nm and for the DSPE-PEG-DBCO-Cy3 with 5000 Da PEG this is a size of approximately 300 nm.

Table 4.2: The hydrodynamic size and PDI of the LNPs made with post-insertion of DSPE-PEG-DBCO-Cy3 batch 2 measured with DLS. Various samples, shown in light gray, have insufficient LNPs in the sample to be measured by DLS. These measurements are not reliable. The number average (nm) is shown.

	Hydrodynamic size (nm)
LNP (before spinfiltration)	387.8 ± 58.9
LNP	335.4 ± 76.3
LNP DSPE-PEG2000-DBCO-Cy3 0.1%(before spinfiltration)	437.3 ± 62.1
LNP DSPE-PEG2000-DBCO-Cy3 0.1%	344.3 ± 79.3
LNP DSPE-PEG2000-DBCO-Cy3 0.2% (before spinfiltration)	472.2 ± 72.5
LNP DSPE-PEG2000-DBCO-Cy3 0.2%	294.7 ± 51.9
LNP DSPE-PEG2000-DBCO-Cy3 0.3%	566.1 ± 118.9
DSPE-PEG2000-DBCO-Cy3 0.2% (before spinfiltration)	939.4 ± 182.8
LNP DSPE-PEG5000-DBCO-Cy3 0.1%	555.6 ± 118.6
LNP DSPE-PEG5000-DBCO-Cy3 0.2%	858.0 ± 69.2
LNP DSPE-PEG5000-DBCO-Cy3 0.3%	327.8 ± 50.9
DSPE-PEG5000-DBCO-Cy3 0.2% (before spinfiltration)	319.3 ± 78.1
LNP Cy3-PEG-SH 0.1 %	358.7 ± 94.1
LNP Cy3-PEG-SH 0.2 %	227.3 ± 60.8
LNP Cy3-PEG-SH 0.3 %	392.7 ± 117.7

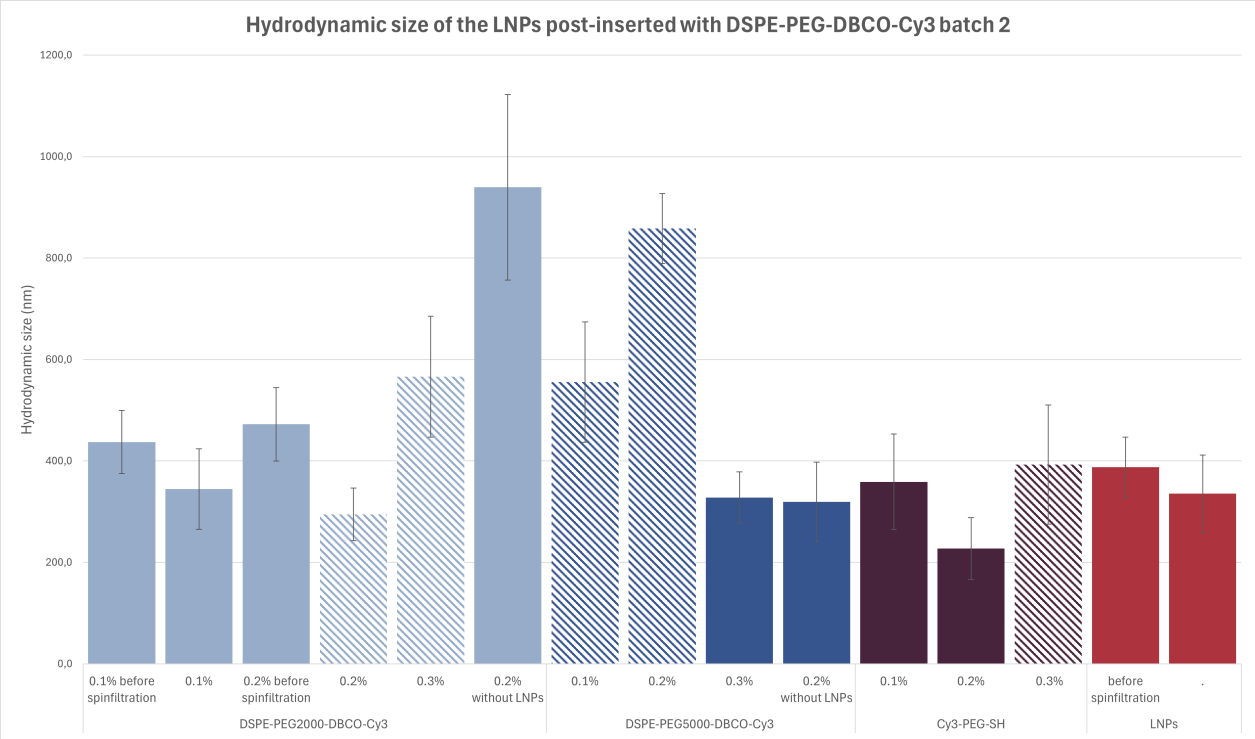

Figure 4.4: The hydrodynamic size of the LNPs post-inserted with DSPE-PEG-DBCO-Cy3 of batch 2, with values from table 4.2. The striped bars have insufficient LNPs to be measured by DLS and are not reliable.

4.4.2 Post-insertion DSPE-PEG-DBCO-Cy3 Batch 3

Figure 4.5 shows the Cy3 fluorescence of the post-insertion with DSPE-PEG-DBCO-Cy3 into the LNPs. DSPE-PEG-DBCO-Cy3 with 2000 Da PEG shows an overall lower fluorescence than DSPE-PEG-DBCO-Cy3 with 5000 Da PEG. So more DSPE-PEG-DBCO-Cy3 with 5000 Da PEG are post-inserted into the LNPs. DSPE-PEG-DBCO-Cy3 with 2000 and 5000 Da PEG shows an increase in fluorescence with an increase in molar ratio. The control with only Cy3-PEG-SH dye shows a low fluorescence for all three molar ratios. The control with only LNPs in the sample shows no fluorescence. The control sample with only DSPE-PEG-DBCO-Cy3 with 2000 Da PEG shows almost no fluorescence. However, the control with only DSPE-PEG-DBCO-Cy3 with 5000 Da PEG shows a very high fluorescence of approximately 15000. This is not as expected since there are no LNPs present in the sample.

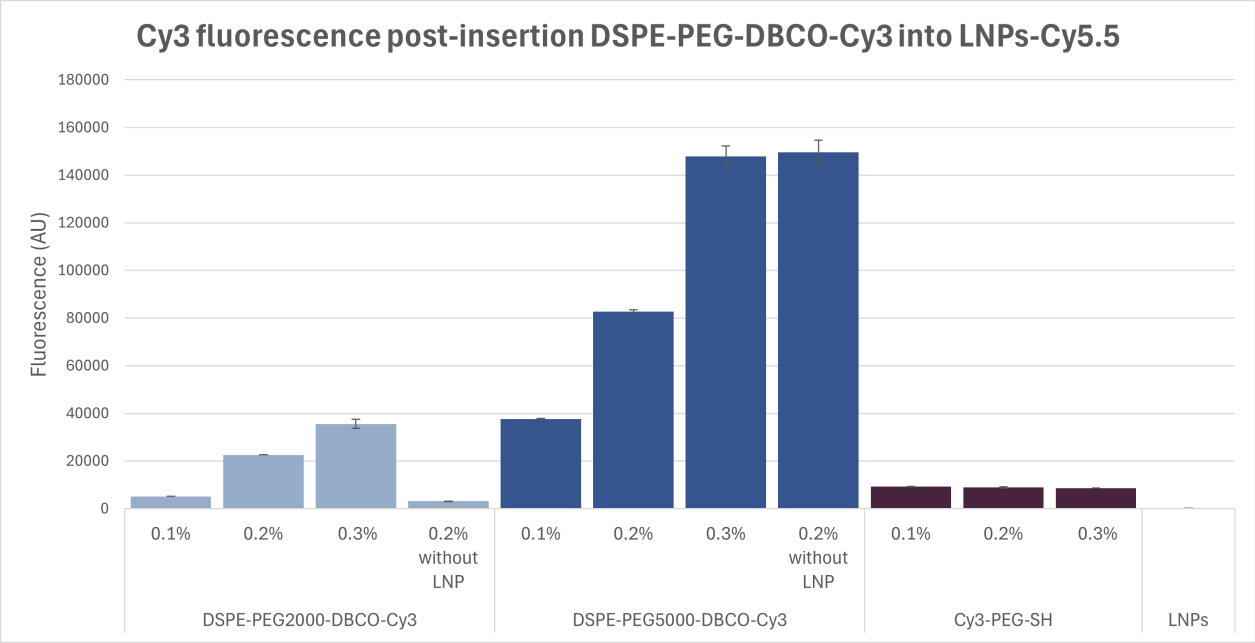

Figure 4.5: The Cy3 fluorescence of the post-insertion with DSPE-PEG-DBCO-Cy3 into the LNPs, batch 3.

The LNPs are measured with DLS on size, the results can be seen in table 4.3. To get a better visualization the same results are put in a graph in figure 4.6. The size of the LNPs stays approximately the same for the post-insertion with DSPE-PEG-DBCO-Cy3 with 2000 Da PEG for 0.1 and 0.2 %. However, there is a large increase in size for the LNPs post-inserted with DSPE-PEG-DBCO-Cy3 with 2000 Da PEG 0.3 % and all the DSPE-PEG-DBCO-Cy3 with 5000 Da PEG. The control samples with only Cy3-PEG-SH dye show a similar size as the LNPs without post-insertion. The control samples with only DSPE-PEG-DBCO-Cy3 present and no LNPs show that there are indeed particles present, which is not as expected since there are no LNPs added to this sample. For the DSPE-PEG-DBCO-Cy3 with 2000 Da PEG a size of approximately 900 nm and the DSPE-PEG-DBCO-Cy3 with 5000 Da PEG a size of approximately 400 nm.

Table 4.3: The hydrodynamic size and PDI of the LNPs made with post-insertion of DSPE-PEG-DBCO-Cy3 batch 3 measured with DLS. The number average (nm) is shown.

	Hydrodynamic size (nm)
LNP	283.6 ± 59.6
LNP DSPE-PEG2000-DBCO-Cy3 0.1%	322.1 ± 84.3
LNP DSPE-PEG2000-DBCO-Cy3 0.2%	227.3 ± 63.65
LNP DSPE-PEG2000-DBCO-Cy3 0.3%	544.3 ± 84.2
DSPE-PEG2000-DBCO-Cy3 0.2%	917.7 ± 137.3
LNP DSPE-PEG5000-DBCO-Cy3 0.1%	576.5 ± 92.9
LNP DSPE-PEG5000-DBCO-Cy3 0.2%	488.0 ± 110.5
LNP DSPE-PEG5000-DBCO-Cy3 0.3%	568.5 ± 82.6
DSPE-PEG5k-DBCO-Cy3 0.2%	419.1 ± 83.32
LNP Cy3-PEG-SH 0.1 %	261.9 ± 49.3
LNP Cy3-PEG-SH 0.2 %	316.0 ± 62.5
LNP Cy3-PEG-SH 0.3 %	307.9 ± 68.73

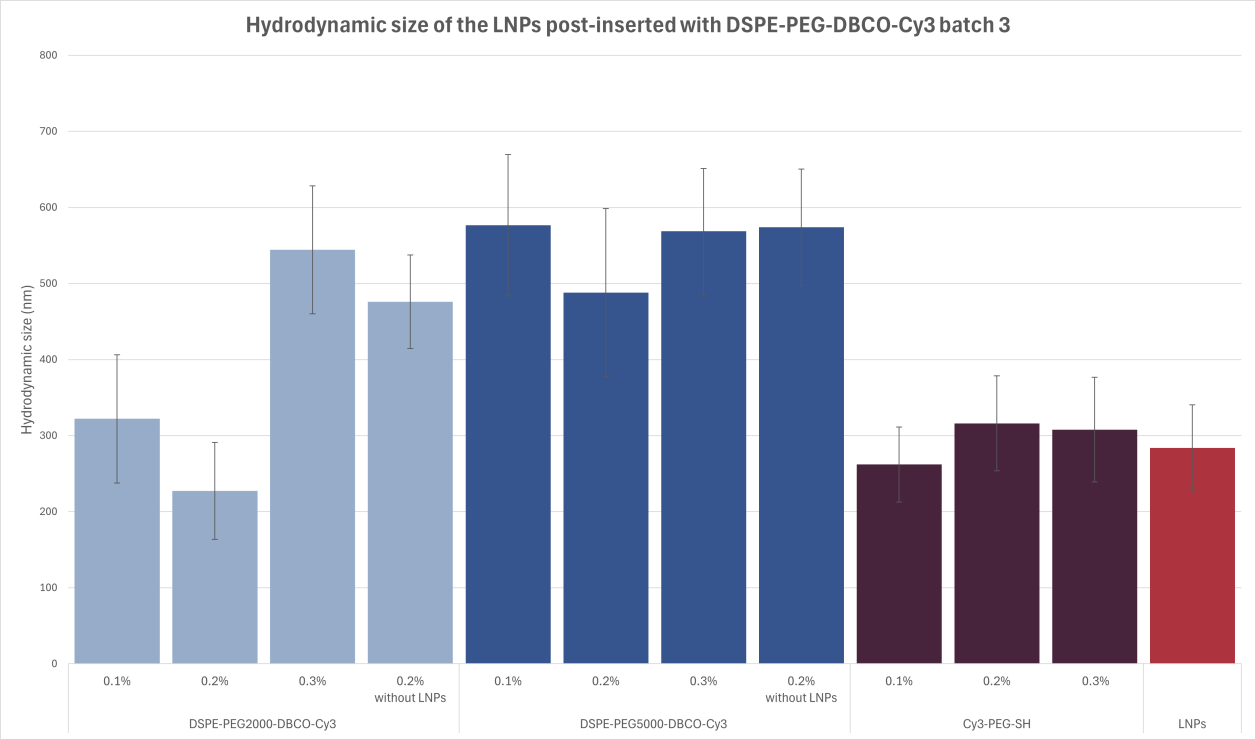

Figure 4.6: The hydrodynamic size of the LNPs post-inserted with DSPE-PEG-DBCO-Cy3 of batch 3, with values from table 4.3.

Comparing batch 2 and 3 of post-insertion with DPSE-PEG-DBCO-Cy3 into the LNPs, figure 4.3 and 4.5, the same trends can be seen. With a higher molar ratio of DSPE-PEG-DBCO-Cy3 with 2000 and 5000 Da PEG, a higher fluorescence can be seen. Implying more lipids post-inserted into the LNPs. The fluorescence of DSPE-PEG-DBCO-Cy3 with 5000 Da PEG is higher than DSPE-PEG-DBCO-Cy3 with 2000 Da PEG. The control samples with only Cy3-PEG-SH added with the LNPs show almost no fluorescence for both batches, meaning that the Cy3-PEG-SH does not interact non-specific with the LNPs and is filtered out of the membranes during dialysis.

When comparing the sizes of the LNPs of the post-insertion with DSPE-PEG-DBCO-Cy3, figure 4.4 and 4.6, differences can be seen between the batches. The LNPs without post-insertion show a size of 335.4 $\pm$ 76.3 for batch 2 and 283.6 $\pm$ 59.6 for batch 3, this difference is minimal. The size of the LNPs post-inserted with DSPE-PEG-DBCO-Cy3 with 2000 Da PEG 0.1%, show a similar size for both batches around 330 nm. The size of the LNPs post-inserted with DSPE-PEG-DBCO-Cy3 with 2000 PEG 0.2 and 0.3% cannot be compared, since the results are not reliable for batch 2. The same applies to the post-insertion with DSPE-PEG-DBCO-Cy3 with 5000 PEG 0.1 and 0.2%. The size of the LNPs post-inserted with DPSE-PEG-DBCO-Cy3 with 5000 PEG 0.3%, are much higher for batch 2 than batch 3. Batch 2 shows a size of around 330 nm and batch 3 shows a size of around 570 nm. The LNPs with Cy3-PEG-SH show not a significant difference in size between both batches and compared to the LNPs without post-insertion. Overall, the size of the LNPs increases by post-insertion with a bigger increase for DSPE-PEG-DBCO-Cy3 with 5000 Da PEG than with 2000 Da PEG.

All the post-insertion experiments performed with DSPE-PEG-DBCO-Cy3 show an increase in the size of the LNPs with Cy3-PEG-SH compared to the LNPs without post-insertion, as shown in table A.2, 4.2 and 4.3. This could mean that the dye is interacting non-specific via hydrophobic interactions with the LNPs. However, this size is still comparable to the LNPs without post-insertion, since the standard deviations are relatively big.

For the post-insertion with DSPE-PEG-Mal/DBCO-Cy3 into the LNPs, the concentration of DSPE-PEG-Mal/DBCO-Cy3 is calculated using a calibration curve with known concentrations. This calculated concen-

tration is an estimate of the real concentration. However, this estimate is reliable, since the ratios between the tested molar ratios stay the same. Only the exact molar ratios of the lipids can be off, which can influence the post-insertion of these lipids, by for example inserting less or more lipids into the LNPs.

The fact that the Cy3-PEG-SH/Azide-PEG2000-Cy3 dye can interact non-specific by hydrophobic interactions with DSPE-PEG-Mal/DBCO draws some concerns for the post-insertion of DSPE-PEG-Mal/DBCO-Cy3. Namely that DSPE-PEG-Mal/DBCO-Cy3 can interact with the surface of the LNPs. This means that DSPE-PEG-Mal/DBCO-Cy3 is not inserted into the LNPs, but there is still fluorescence detectable. This would also mean that the size increases more than when post-insertion happens. This effect should be seen more for the DSPE-PEG-Mal/DBCO with 5000 Da PEG than for 2000 Da PEG, since the PEG spacer is longer. Another interaction that could happen is the coupling of two LNPs with each other. If the hydrophobic tail of DSPE-PEG-Mal/DBCO-Cy3 is inserted in the LNP and the Cy3 dye part on the surface of the LNP is interacting non-specific by hydrophobic interactions with another LNP.

The mechanism of post-insertion is that the hydrophobic tail of DSPE-PEG-Mal/DBCO-Cy3 is inserted into the LNPs. But the Cy3 dye side of this molecule is also hydrophobic. There is not looked at the possibility that the molecule is inserted upside down, so the Cy3 side is inserted into the LNP. This does not influence the size of the LNPs, since the size of the lipids does not change. To test this phenomenon, a fluorescence microscope could be used to see if the Cy3 fluorescence is present inside the LNP or at the surface of the LNP [75].

The fluorescence values of the post-inserted LNPs are corrected for the amount of particles present in the samples, the Cy3 is divided by the Cy5.5 fluorescence. The assumption is made that all particles have the same amount of Cy5.5 fluorescence. However, as figure A.3b and 4.3b show, the Cy5.5 fluorescence fluctuates for every sample. This variability undermines the assumption. If the Cy5.5 fluorescence is low, indicating fewer particles. the Cy3 fluorescence might still be high due to more insertion of DSPE-PEG-DBCO/Mal-Cy3 into the LNPs. Therefore, the expectation that dividing the Cy3 by Cy5.5 values would not influence the results is contradicted, as fluctuations in the Cy5.5 fluorescence can lead to misleading interpretations of the Cy3 fluorescence signal.

The sizes of all post-inserted LNPs with DSPE-PEG-Mal/DBCO-Cy3 are measured with DLS. This machine is good at measuring small amounts of LNPs, but less good at measuring polydisperse nanoparticles [66]. This is for some samples corrected by taking the number average instead of the z-average. Nanoparticles with a big size scatter more light than nanoparticles with a small size, which results in a higher intensity peak of the big particle than the small particle. The number average corrects for the scattering per nanoparticle difference using mathematical models. This gives a better indication of the size of the nanoparticles. However, a disadvantage is that in this way there is not a PDI shown. But the standard deviation of the size of the LNPs is an indication of the PDI [66]. Instead of using DLS to measure the size and PDI, Nanoparticle Tracking Analysis (NTA) can be used [76]. This is a technique that also uses the Brownian-motion of the particles and calculates the hydrodynamic size of the nanoparticles with the help of the Stokes-Einstein equation. NTA performs better for more polydisperse nanoparticles, as in these experiments.

To get the PDI of the particles lower, the recommendation is made to use spinfilters instead of dialysis for the purification of the LNPs. Table 4.4 shows samples measured before and after spinfiltration. The sample with only LNPs and the sample with LNPs post-inserted with DSPE-PEG-DBCO-Cy3 0.1% both show a decrease in size after spinfiltration. This is caused by the centrifugal force that breaks up the aggregates of the nanoparticles.

The fluorescence of the post-inserted LNPs with DSPE-PEG-DBCO-Cy3 with 5000 Da PEG show a higher value than DSPE-PEG-DBCO-Cy3 with 2000 Da PEG. As can be seen in figure 4.3a and 4.5. This could mean that DSPE-PEG-DBCO-Cy3 with 5000 Da PEG are build in more than DSPE-PEG-DBCO-Cy3 with 2000 Da PEG. The probable cause for this is that the PEG spacer is longer of DSPE-PEG-DBCO-Cy3 with 5000 Da PEG and builds in more easily since it causes less steric hindrance since the Cy3 dye molecule is further away from the surface of the LNP. However, this could also mean that the size increases more of the

LNPs, since that Cy3 dye molecule is further away from the LNP surface, this can indeed be seen in table 4.3.

Table 4.2, 4.3 and 4.4 show particles present in the samples without LNPs. The size for the post-inserted LNPs with DSPE-PEG-Mal/DBCO-Cy3 with 2000 Da PEG is every time around 900 nm, and for the post-inserted LNPs with DSPE-PEG-Mal/DBCO-Cy3 with 5000 Da PEG around 300-400 nm. The samples have a high PDI for every measurement. One reason for the detection of particles could be that the samples are too polydisperse and the DLS machine cannot measure it correctly. Another reason could be the formation of micelles, since the samples only contain DSPE-PEG-Mal/DBCO-Cy3 which can interact with each other by hydrophobic interactions and form micelles [12].

4.5 Conjugation DSPE-PEG-Mal to VHH

4.5.1 Batch 1

In figure 4.7 the result of the SDS-page is shown of the conjugation with the DSPE-PEG-Mal with 5000 Da PEG to the VHHs. It can be seen that every lane has a band at 15 kDa, this is the band of the VHH. The lane of DSPE-PEG-Mal-VHH with 5000 Da PEG shows a band at 25 kDa, shown with the black arrow, this is the molecular weight of the conjugated DSPE-PEG-Mal with 5000 Da PEG to VHH. The green arrows do not show these bands, these are the control lanes of DSPE-PEG-Mal-blocked and 8-arm-PEG-Mal. The 8-arm-PEG-Mal shows multiple bands in the region of 100-150, shown with the blue arrow. These bands are related to the 8-arm-PEG-Mal conjugated to multiple VHHs (4-8). The band at 25 kDa, showing DSPE-PEG-Mal-VHH with 5000 Da PEG, has a relatively low intensity. This is because the VHHs were not reduced with TCEP before reacting with DSPE-PEG-Mal.

The bands are quantified on the efficiency of the conjugation. This measurement did not have a sample with only VHH, so the assumption is that a 32.5% loss, as calculated from batch 2, has occurred. The lane with DSPE-PEG-Mal with 5000 Da PEG conjugated to VHH shows a band of 37.8% at 15 kDa and a band of 29.8% at 25 kDa. The lane with the DSPE-PEG-Mal with 5000 Da PEG blocked shows a band at 15 kDa of 67.5%. The lane with the 8-arm-PEG-Mal shows a band at 15 kDa of 26.3% and a bands at 100-150 kDa add up to 41.3%. Summarizing, the conjugation efficiency of the VHHs to DSPE-PEG-Mal with 5000 Da PEG is approximately 29.8%, which is approximately 10% less compared to the positive control 8-arm-PEG-Mal. Blocking of the maleimide was effective, resulting in no conjugation, showing that no non-specific binding is occurring between the VHHs and DSPE-PEG-Mal.

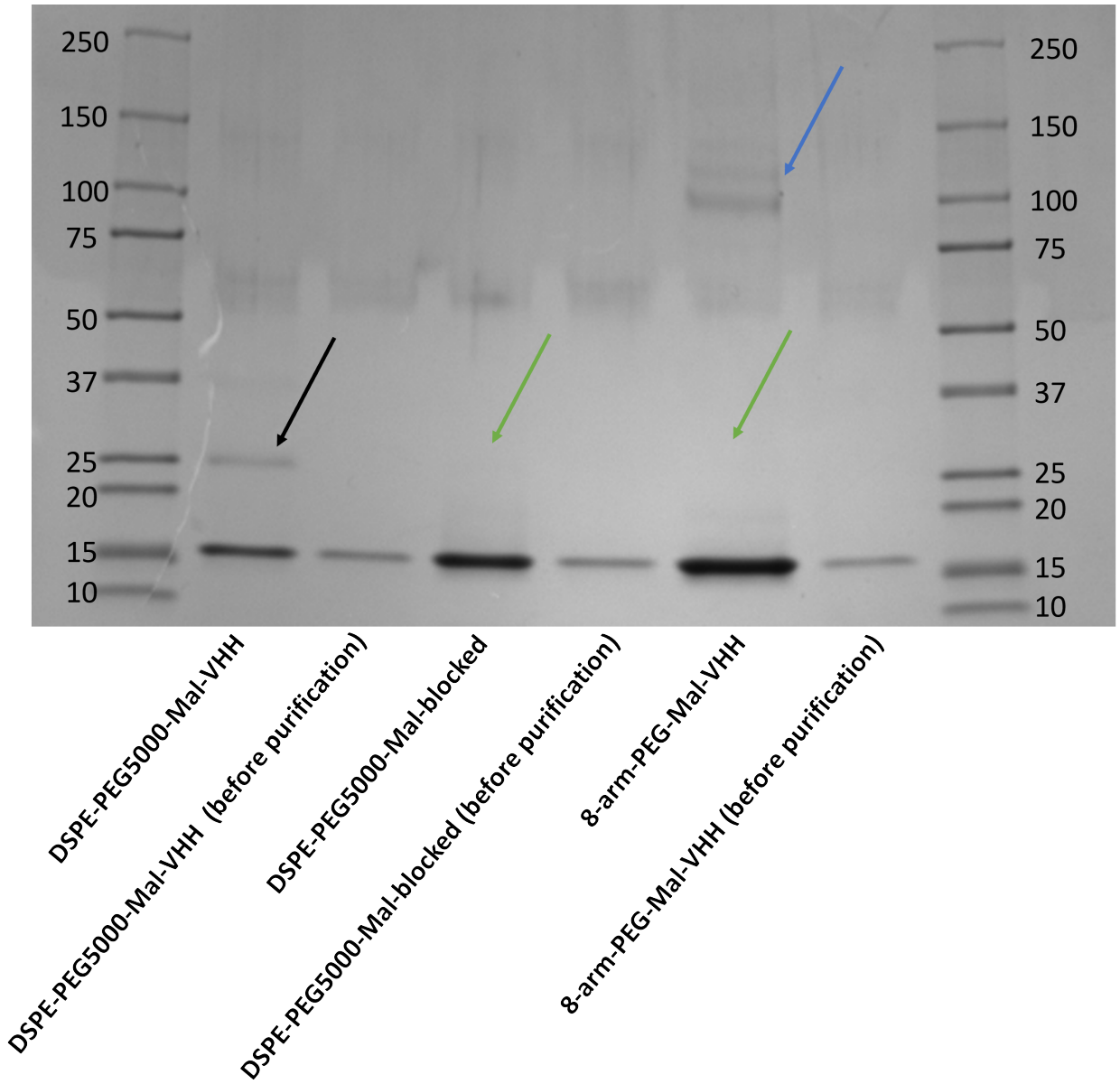

Figure 4.7: The SDS-page of the conjugation of DSPE-PEG-Mal to the VHHs, batch 1.

4.5.2 Batch 2

Figure 4.8 shows the result of the SDS-page of the repeated conjugation with DSPE-PEG-Mal with 5000 Da PEG to the VHHs. Before conjugation, TCEP was left to react with the VHHs as reducing agent between VHHs. The black arrow points to a band at a molecular weight of 25 kDa, this is the DSPE-PEG-Mal with 5000 Da PEG conjugated to the VHH. The control samples do not show these bands, shown by the green arrows. The 8-arm-PEG-Mal, taken as positive control, reacted with the VHHs. This can be seen by the blue arrows, pointing at multiple bands around 100-150 kDa.

The bands are quantified on the efficiency of the conjugation. The band with only VHH is set to 100%. The lane with DSPE-PEG-Mal with 5000 Da PEG conjugated to VHH shows a band at 15 kDa of 34.4% and a band at 25 kDa of 31.4%, this means a loss of 34.2%. The lane with DSPE-PEG-Mal with 5000 Da PEG blocked shows a band at 15 kDa of 67.2%, with a loss of 32.8% for this sample. The lane with the 8-arm-PEG-Mal shows a band at 15 kDa of 20.1%, and the three bands together at 100-150 kDa add up to 47.3%. This sample has a loss of 32.6%. Summarizing, the samples show an overall loss of around 30-35%. The conjugation of DSPE-PEG-Mal with 5000 Da PEG to the VHH has an efficiency of 31.4%.

Summarizing, the conjugation efficiency of this VHH with DSPE-PEG-Mal with 5000 Da PEG is approximately 31.4%, which is approximately 15% less compared to the positive control 8arm-PEG-Mal. Blocking of the maleimide was effective, resulting in no conjugation, showing that no non-specific binding is occurring between the VHHs and DSPE-PEG-Mal.

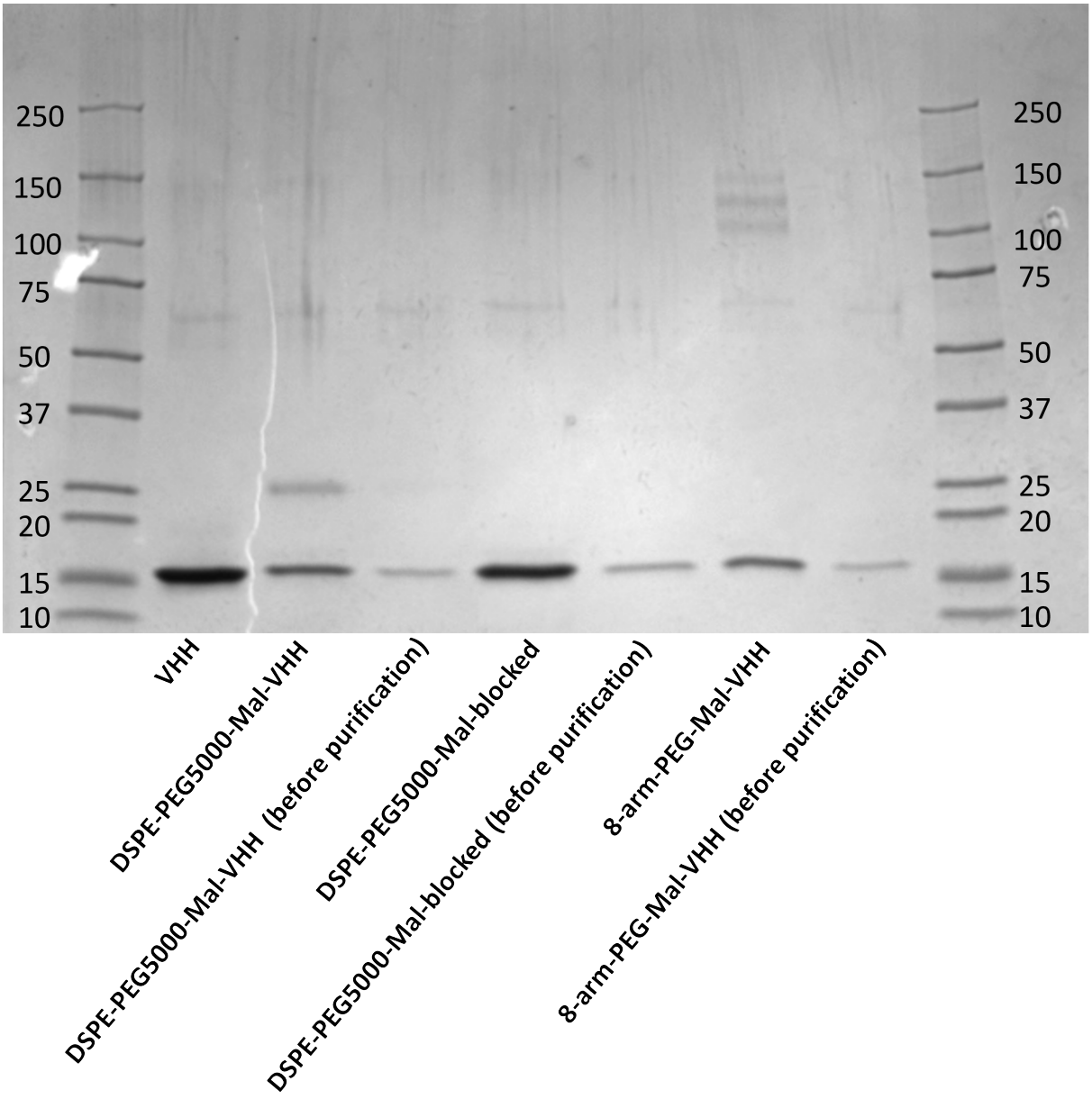

Figure 4.8: The SDS-page of the conjugation with DSPE-PEG-Mal with 5000 Da PEG to the VHHs, batch 2.

Evaluating the effect of TCEP on the conjugation efficiency shows that reducing the VHHs with TCEP has no significant effect. However, this might not be the case. The efficiency of batch 1 is calculated with the help of the calculated loss of batch 2, since batch 1 does not have a lane with only VHHs. Batch 1 can have a higher or lower loss, if the loss is lower, the conjugation efficiency would be higher and vice versa. So TCEP could indeed reduce the VHHs and play a bigger role than shown here if the loss is more. For future experiments, the conjugation needs to be performed again with and without reducing the VHHs with TCEP, to research if reducing with TCEP results in a higher conjugation efficiency. For this, a sample with only VHHs should be taken into account and undergo the same steps according to section 3.2.5. This lane can be compared to the lane with VHHs that did not undergo the steps to get a better look at how the loss of approximately 30-35% happens and if it happens during the conjugation or SDS-page analysis.

The quantification of the conjugation of DSPE-PEG-Mal with 5000 Da PEG to the VHHs shows clear results for both batches. The conjugation succeeded with an efficiency of approximately 30% and the blocked DSPE-PEG-Mal with 5000 Da PEG does not show conjugation. 8-arm-PEG-Mal, as positive control, shows conjugation to multiple VHHs with an efficiency of approximately 43%. However, the conjugation efficiency is still quite low. For all reactions DSPE-PEG-Mal with 5000 Da PEG reacted with the VHHs in a molar ratio of 5:1. The coupling of the VHHs to maleimide groups has been shown by Lin Zhong performed with polymers in a molar ratio of 10:1 [77]. Recommended is to perform the experiments again, with a molar ratio of 10:1. If that still causes a low conjugation efficiency, an even higher molar ratio of DSPE-PEG-Mal can be tested, since the unconjugated DSPE-PEg-Mal are washed out during the purification steps.

4.6 Post-insertion DSPE-PEG-Mal-VHH

Figure 4.9 shows the result of the post-inserted LNPs with DSPE-PEG-Mal-VHH with 5000 Da PEG. The control sample with only VHH shows a band at 15 kDa. The red arrow points to a band of a lower intensity around 60 kDa. The samples with 0.1% DSPE-PEG-Mal-VHH with 5000 Da PEG show no bands at 15 and 25 kDa. The samples with 0.2% DSPE-PEG-Mal-VHH with 5000 Da PEG show a band at 15 kDa at a very low intensity, but not a band at 25 kDa. The sample with 0.3% DSPE-PEG-Mal-VHH with 5000 Da PEG shows a band with low intensity at 15 kDa and 25 kDa. This sample shows the same band around 60 kDa as the sample with only VHH, but at a higher intensity. The sample with only DSPE-PEG-Mal-VHH with 5000 Da PEG at 0.2% molar ratio shows a band at 15 kDa and 25 kDa. The control sample with LNPs shows no band at 25 kDa.

The SDS-page of the post-insertion with DSPE-PEG-Mal-VHH, figure 4.9, shows a band around 60 kDa for the sample with VHHs and the sample with DSPE-PEG-Mal-VHH 0.3%. This band can also be seen in all the samples of the conjugation of DSPE-PEG-Mal to the VHHs in figure 4.8 and vaguely in figure 4.7. First, there is speculated that DSPE-PEG-Mal-VHH could form micelles, however this is contradicted since the sample with only VHH and no DSPE-PEG-Mal-VHH in figure 4.9 does not show this band. Another explanation for the 60 kDa band is that the VHHs aggregated. Usually this would not happen since the VHHs are stored in PBS as solvent in the freezer and the solvent of the experiments is also PBS. However, the VHHs are stored for at least 2 years in the freezer, so this could be an explanation that the VHHs aggregated together.

In the SDS-page, the LNPs fall apart so the separate lipids are measured. The assumption is made that the non-inserted DSPE-PEG-Mal-VHH are washed away during spinfiltration. However, spinfilters with a 10 kDa MWCO instead of 30 kDa MWCO were used. This means that the non-inserted DSPE-PEG-Mal-VHH of approximately 25 kDa are not washed out of the samples. The results are therefore unreliable, because DSPE-PEG-Mal-VHH which are seen on the SDS-page can be post-inserted into the LNPs or floating freely in the sample.

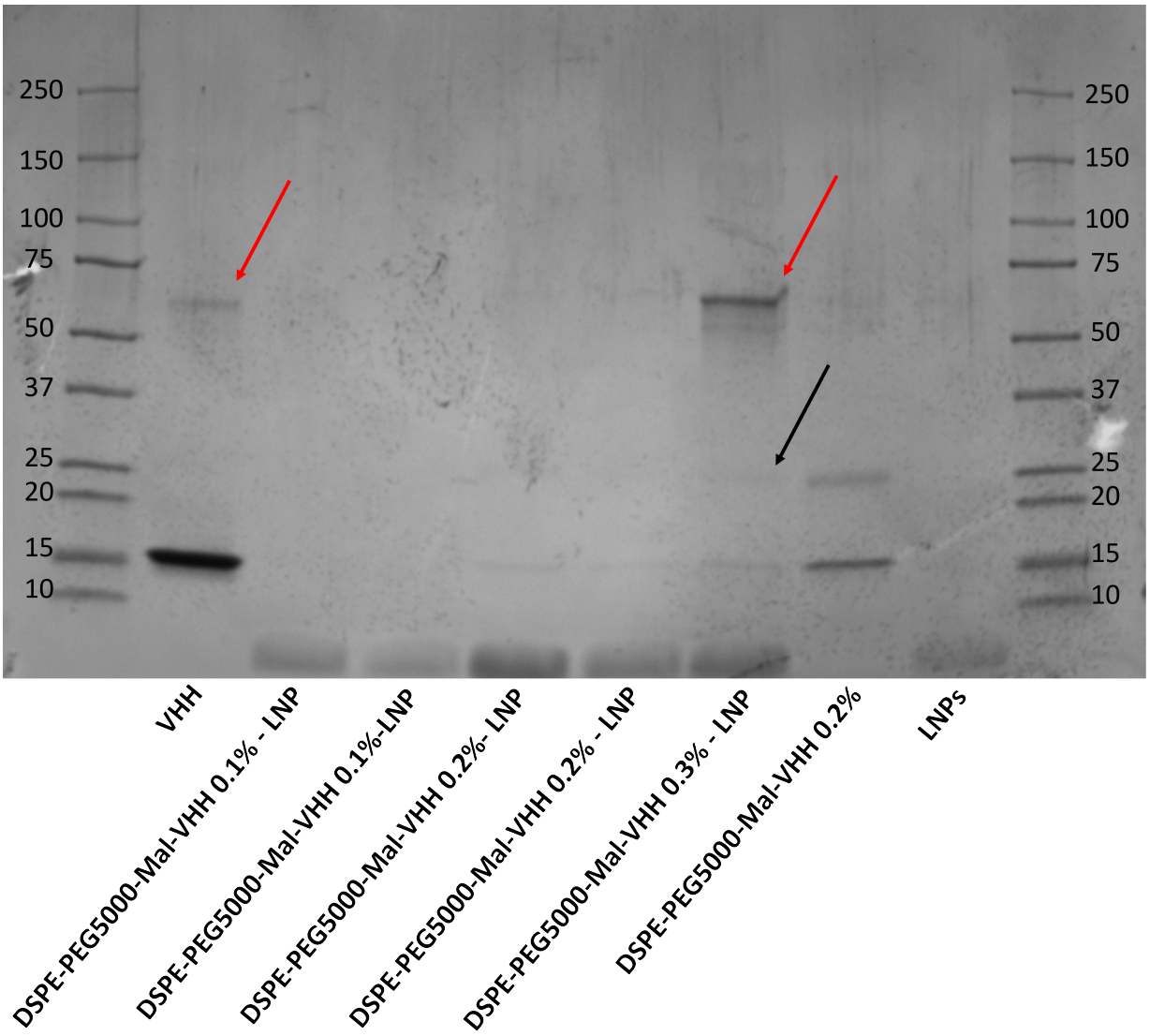

Figure 4.9: The SDS-page of the post-insertion with DSPE-PEG-Mal-VHH with 5000 Da PEG into LNPs.

Table 4.4 shows the size and PDI of the post-inserted LNPs with DSPE-PEG-Mal-VHH with 5000 Da PEG, measured with DLS. Figure 4.10 visualizes the result in a graph. These results are still reliable, since the DLS measures the particles and not the separate DSPE-PEG-Mal-VHH lipids. The post-inserted LNPs show a similar size as the LNPs without any post-insertion of approximately 120-130 nm, for all molar ratios. The standard deviation of all post-inserted LNPs is very low, with a few nanometers. In the control sample with only DSPE-PEG-Mal-VHH with 5000 Da PEG, there are particles present and detected by the DLS measurements of approximately 800 nm with a high PDI.

Table 4.4: The hydrodynamic size and PDI of the LNPs made with post-insertion of DSPE-PEG-Mal-VHH with 5000 Da PEG measured with DLS, the Z-average (nm) is shown.

	Hydrodynamic size (nm)	**Polydispersity Index (PDI)**
LNPs	129.1 ± 0.4	0.196
LNP DSPE-PEG5000-Mal-VHH 0.1%	128.8 ± 3.3	0.151
LNP DSPE-PEG5000-Mal-VHH 0.1%	121.5 ± 0.5	0.143
LNP DSPE-PEG5000-Mal-VHH 0.2%	120.7 ± 1.4	0.138
LNP DSPE-PEG5000-Mal-VHH 0.2%	120.7 ± 1.7	0.153
LNP DSPE-PEG5000-Mal-VHH 0.3%	124.8 ± 0.4	0.174
DSPE-PEG5000-Mal-VHH 0.2 %	325.0 ± 170.4	0.804

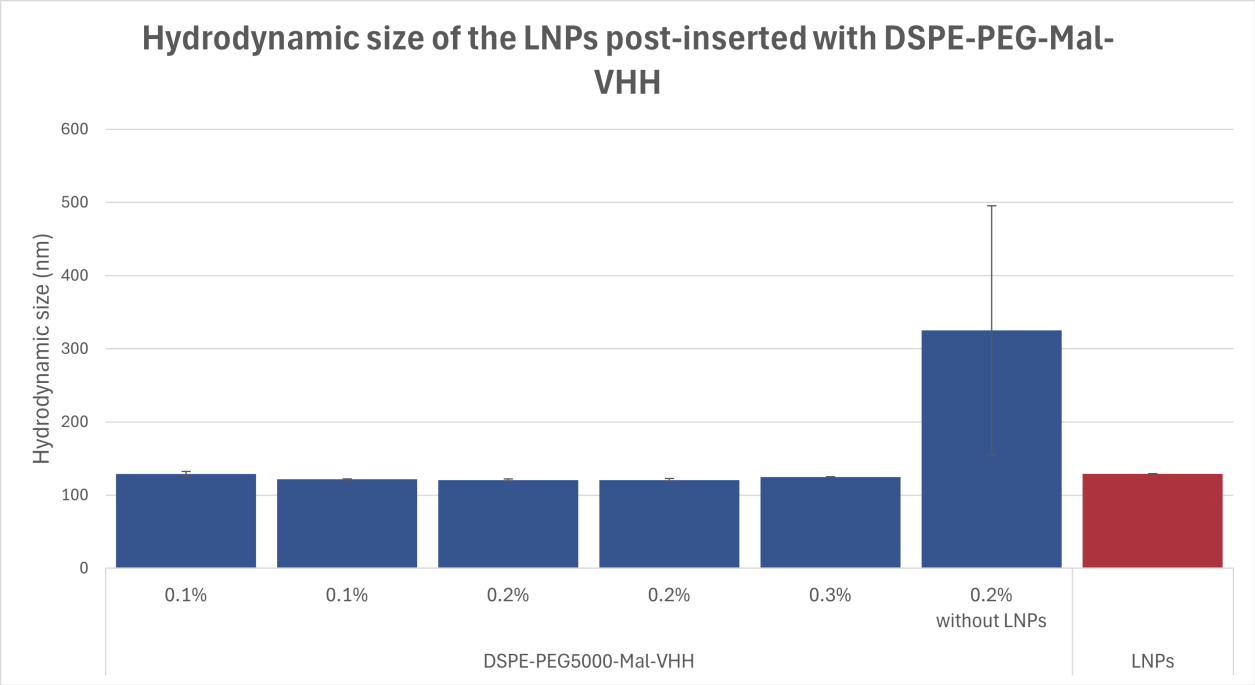

Figure 4.10: The hydrodynamic size of the LNPs post-inserted with DSPE-PEG-Mal-VHH with 5000 Da PEG. The values of table 4.4 are visualised.

Evaluating the post-insertion results with DSPE-PEG-Mal-VHH, the amount of DSPE-PEG-Mal-VHH inserted into the LNPs is not determined. To achieve this information, a calibration curve could be made. By measuring various concentrations of DSPE-PEG-Mal-VHH on an SDS-page and measuring the intensity of the bands. If the SDS-page with the post-inserted LNPs is performed, the calibration curve can be used to find the concentration of DSPE-PEG-Mal-VHH inserted into the LNPs.

Another possibility is to label the VHHs with a fluorescent dye. In that case, the results of the post-insertion of DSPE-PEG-Mal-VHH into the LNPs do not need to be quantified using an SDS-page but a simple fluorescence measurement with the Varioskan LUX 3020-528 from Thermofisher is sufficient, this will be less time-consuming. For example, a FITC-NHS dye could be used to label the VHHs [78]. By giving the VHHs a fluorescent label, the placement of the inserted DSPE-PEG-Mal-VHH can be seen with the help of a fluorescence microscope.

By knowing the concentration of DSPE-PEG-Mal-VHH, the amount of VHHs on the outside of the LNP can be determined. This is important since it is not yet known how many VHHs are needed on the outside of the LNPs to get them to the target cells. By knowing the amount of VHHs on the outside, the LNPs can be added to cells and tests can be performed to achieve the best VHH concentration to receive the highest targeting. This is for future research, since the post-insertion of the DSPE-PEG-Mal-VHH first needs to be confirmed.

For future research, the purification of the samples with LNPs post-inserted with DSPE-PEG-Mal-VHH with 5000 Da PEG should be performed with 30 kDa MWCO spinfilters instead of 10 kDa MWCO spinfilters, to wash the non-inserted DSPE-PEG-Mal-VHH out of the sample. Also, higher concentrations of the samples need to be put into the SDS-page gels, since the bands of the lipids are barely detectable. The recommendation is to use 5 μg instead of 2 μg.

All experiments are performed once, with n=1. To make the results significant and more reliable, the experiments need to be performed at least 3 times (n=3) [79].

The LNPs are measured on size and PDI with DLS. The morphology of the LNPs has not been looked

at. Because of the post-insertion, the morphology of the LNPs can change. The morphology can be looked at using a fluorescent microscope, for example, using a fluorescence-based confocal laser scanning microscope [75]. In this way, the Cy5.5 of the LNPs can be seen to ensure the presence of LNPs. The Cy3 fluorescence signal can also be seen, this should be a 'shield' around the surface of the LNPs, if DSPE-PEG-Mal/DBCO-Cy3 are post-inserted correctly into the LNPs. This microscopic method to look at the morphology of the LNPs can also be used for DSPE-PEG-Mal-VHH. However, the VHHs need to be labeled with a fluorescent dye, as mentioned above. Instead of DLS, NTA should be used to measure the size and PDI of the LNPs, since it is more suitable for more polydisperse nanoparticles [76]. Another characteristic to look at is the surface charge of the LNP, so the Zeta-potential which is measured with DLS. By measuring these 2 properties, a better overview of the properties of the LNPs can be given. This information can be helpful to know how the LNPs will react in the body when interacting with the cells.

Eventually, the goal is to deliver LNPs to target cells in the body, so that they can deliver the drugs to the cells. Yetisgin et al. showed that nanoparticles should have a size of <200 nm to be the most effective in drug delivery [22]. As shown in table A.1 and table A.2, the LNPs post-inserted with DSPE-PEG-Mal/DBCO-Cy3 show a high PDI and a large increase in size. To use these particles for targeted drug delivery, they need to decrease in size. So the methods of the post-insertion still need to be optimized.

Chapter 5

Conclusion

Summarising, the conjugation of both the DSPE-PEG-Mal and DSPE-PEG-DBCO to Cy3-PEG-SH and Azide-PEG2000-Cy3 are successful. The conjugation of DSPE-PEG-DBCO/Mal with 5000 Da PEG shows a higher fluorescence than DSPE-PEG-DBCO/Mal with 2000 Da PEG, so a higher conjugation is achieved. However, the high fluorescence in the blocked DSPE-PEG-Mal/DBCO samples can be caused by non-specific hydrophobic interactions or the blocking not working properly. The conjugation of DSPE-PEG-Mal-with 5000 Da PEG to VHHs succeeded, reducing the VHHs with TCEP results in a higher conjugation efficiency of 31.4%.

The results of the post-insertion with DSPE-PEG-Mal-Cy3 are inconclusive. The post-insertion with DSPE-PEG-DBCO-Cy3 shows more fluorescence for the DSPE-PEG-DBCO-Cy3 with 5000 Da PEG than DSPE-PEG-DBCO-Cy3 with 2000 Da PEG, so more lipids are inserted into the LNPs when using a longer PEG-linker. The post-insertion leads overall to a larger size and a larger PDI. A higher molar ratio of DSPE-PEG-Mal/DBCO-Cy3 results in more fluorescence, so more lipids are inserted into the LNPS. A higher molar ratio of DSPE-PEG-Mal/DBCO-Cy3 does not influence the size of the LNPs. The post-insertion of DSPE-PEG-Mal-VHH with 5000 Da PEG is inconclusive, because the non-inserted DSPE-PEG-Mal-VHH with 5000 Da PEG are not washed out of the sample, and therefore no discrimination could be made between incorporated and loose DSPE-PEG-Mal-VHH on SDS-PAGE. The size and PDI show no change when compared to the LNPs without post-insertion.

Concluding, post-insertion shows promise to be used in the future for targeted drug delivery. DSPE-PEG-Mal/DBCO-Cy3 are inserted into the LNPs and DSPE-PEG-DBCO with 5000 Da PEG 0.3% molar ratio shows the best results. Recommended is to look further into the post-insertion with DSPE-PEG-Mal-VHH, since the size and PDI of the LNPs do not increase, showing this as a promising strategy for conjugating LNPs with VHHs.

Chapter 6

Acknowledgements

Firstly, I would like to thank Prof. Dr. H.B.J. Karperien for being my committee chair and giving me valuabe input and feedback on my bachelor's assignment.

I am also thankful to Dr. R. Bansal for being my external supervisor and providing valuable input and feedback on my bachelor's assignment.

Furthermore, I want to thank Dr. B. Zoetebier and Dr. J. Hendriks for being my daily supervisors and guiding me through my bachelor's assignment.

Lastly, I would like to acknowledge and thank everyone at the DBE group for their assistance, moral support, and warm welcome. With a special thanks to Jamie Kossen for her support and guidance in the labs.

References

[1] S. Aboulenain and A. Y. Saber. "Primary Osteoarthritis". In: *StatPearls [Internet]*. StatPearls Publishing, 2022. URL: https://www.ncbi.nlm.nih.gov/books/NBK557808.

[2] G. 2. O. Collaborators. "Global, regional, and national burden of osteoarthritis, 1990–2020 and projections to 2050: a systematic analysis for the Global Burden of Disease Study 2021". In: *Lancet. Rheumatology* 5.9 (2023), e508. DOI: 10.1016/S2665-9913(23)00163-7.

[3] E. Sanchez-Lopez, R. Coras, A. Torres, N. E. Lane, and M. Guma. "Synovial inflammation in osteoarthritis progression". In: *Nat. Rev. Rheumatol.* 18.5 (2022), p. 258. DOI: 10.1038/s41584-022-00749-9.

[4] S. Jang, K. Lee, and J. H. Ju. "Recent Updates of Diagnosis, Pathophysiology, and Treatment on Osteoarthritis of the Knee". In: *Int. J. Mol. Sci.* 22.5 (2021). DOI: 10.3390/ijms22052619.

[5] A. Tewabe, A. Abate, M. Tamrie, A. Seyfu, and E. A. Siraj. "Targeted Drug Delivery — From Magic Bullet to Nanomedicine: Principles, Challenges, and Future Perspectives". In: *Journal of Multidisciplinary Healthcare* 14 (2021), p. 1711. DOI: 10.2147/JMDH.S313968.

[6] R. Mashima and S. Takada. "Lipid Nanoparticles: A Novel Gene Delivery Technique for Clinical Application". In: *Curr. Issues Mol. Biol.* 44.10 (2022), p. 5013. DOI: 10.3390/cimb44100341.

[7] A. Yusuf, A. R. Z. Almotairy, H. Henidi, O. Y. Alshehri, and M. S. Aldughaim. "Nanoparticles as Drug Delivery Systems: A Review of the Implication of Nanoparticles' Physicochemical Properties on Responses in Biological Systems". In: *Polymers* 15.7 (2023). DOI: 10.3390/polym15071596.

[8] Z. P. Aguilar. "Chapter 5 - Targeted Drug Delivery". In: *Nanomaterials for Medical Applications*. Walthm, MA, USA: Elsevier, Jan. 2013, pp. 181–234. ISBN: 978-0-12-385089-8. DOI: 10.1016/B978-0-12-385089-8.00005-4.

[9] Y. Eygeris, M. Gupta, J. Kim, and G. Sahay. "Chemistry of Lipid Nanoparticles for RNA Delivery". In: *Acc. Chem. Res.* 55.1 (2022), pp. 2–12. ISSN: 0001-4842. DOI: 10.1021/acs.accounts.1c00544.

[10] L. Wu, X. Li, X. Qian, S. Wang, J. Liu, and J. Yan. "Lipid Nanoparticle (LNP) Delivery Carrier-Assisted Targeted Controlled Release mRNA Vaccines in Tumor Immunity". In: *Vaccines* 12.2 (2024), p. 186. ISSN: 2076-393X. DOI: 10.3390/vaccines12020186.

[11] L. Xu, X. Wang, Y. Liu, G. Yang, R. J. Falconer, and C.-X. Zhao. "Lipid Nanoparticles for Drug Delivery". In: *Adv. NanoBiomed Res.* 2.2 (2022), p. 2100109. ISSN: 2699-9307. DOI: 10.1002/anbr.202100109.

[12] L. E. Swart et al. "A robust post-insertion method for the preparation of targeted siRNA LNPs". In: *Int. J. Pharm.* 620:121741. (2022). ISSN: 1873-3476. DOI: 10.1016/j.ijpharm.2022.121741. eprint: 35421533.

[13] L. Schoenmaker et al. "mRNA-lipid nanoparticle COVID-19 vaccines: Structure and stability". In: *Int. J. Pharm.* 601 (2021), p. 120586. ISSN: 0378-5173. DOI: 10.1016/j.ijpharm.2021.120586.

[14] T. I. Chio and S. L. Bane. "Click Chemistry Conjugations". In: *Methods in molecular biology (Clifton, N.J.)* 2078 (2020), p. 83. DOI: 10.1007/978-1-4939-9929-3_6.

[15] W. Alshaer et al. "siRNA: Mechanism of action, challenges, and therapeutic approaches". In: *Eur. J. Pharmacol.* 905 (2021), p. 174178. ISSN: 0014-2999. DOI: 10.1016/j.ejphar.2021.174178.

[16] S. Oliveira, G. Storm, and R. M. Schiffelers. “Targeted Delivery of siRNA”. In: *J. Biomed. Biotechnol.* 2006 (2006). DOI: 10.1155/JBB/2006/63675.

[17] Nitika, J. Wei, and A.-M. Hui. “The Delivery of mRNA Vaccines for Therapeutics”. In: *Life* 12.8 (2022). DOI: 10.3390/life12081254.

[18] L. Lin, K. Su, Q. Cheng, and S. Liu. “Targeting materials and strategies for RNA delivery”. In: *Theranostics* 13.13 (2023), p. 4667. DOI: 10.7150/thno.87316.

[19] S. W. L. Lee et al. “MicroRNA delivery through nanoparticles”. In: *J. Controlled Release* 313 (2019), p. 80. DOI: 10.1016/j.jconrel.2019.10.007.

[20] J. O’Brien, H. Hayder, Y. Zayed, and C. Peng. “Overview of MicroRNA Biogenesis, Mechanisms of Actions, and Circulation”. In: *Front. Endocrinol.* 9:402. (2018). ISSN: 1664-2392. DOI: 10.3389/fendo.2018.00402. eprint: 30123182.

[21] J. Dolai, K. Mandal, and N. R. Jana. “Nanoparticle Size Effects in Biomedical Applications”. In: *ACS Appl. Nano Mater.* 4.7 (2021), pp. 6471–6496. DOI: 10.1021/acsanm.1c00987.

[22] A. A. Yetisgin, S. Cetinel, M. Zuvin, A. Kosar, and O. Kutlu. “Therapeutic Nanoparticles and Their Targeted Delivery Applications”. In: *Molecules* 25.9 (2020). DOI: 10.3390/molecules25092193.

[23] S. Parveen, P. Gupta, S. Kumar, and M. Banerjee. “Lipid polymer hybrid nanoparticles as potent vehicles for drug delivery in cancer therapeutics”. In: *Med. Drug Discov.* 20 (2023), p. 100165. ISSN: 2590-0986. DOI: 10.1016/j.medidd.2023.100165.

[24] *Zeta Potential - an overview | ScienceDirect Topics*. [Online; accessed 3. May 2024]. May 2024. DOI: 10.1016/B978-0-323-91668-4.00002-2.

[25] E. Fröhlich. “The role of surface charge in cellular uptake and cytotoxicity of medical nanoparticles”. In: *Int. J. Nanomed.* 7 (2012), p. 5577. DOI: 10.2147/IJN.S36111.

[26] J. D. Clogston and A. K. Patri. “Zeta Potential Measurement”. In: *Characterization of Nanoparticles Intended for Drug Delivery*. Humana Press, 2011, pp. 63–70. ISBN: 978-1-60327-198-1. DOI: 10.1007/978-1-60327-198-1_6.

[27] M. Nikzamir, A. Akbarzadeh, and Y. Panahi. “An overview on nanoparticles used in biomedicine and their cytotoxicity”. In: *J. Drug Delivery Sci. Technol.* 61 (2021), p. 102316. ISSN: 1773-2247. DOI: 10.1016/j.jddst.2020.102316.

[28] H. N. Jung, S.-Y. Lee, S. Lee, H. Youn, and H.-J. Im. “Lipid nanoparticles for delivery of RNA therapeutics: Current status and the role of in vivo imaging”. In: *Theranostics* 12.17 (2022), p. 7509. DOI: 10.7150/thno.77259.

[29] *DSPE-PEG 2000*. [Online; accessed 10. Jul. 2024]. July 2024. URL: https://www.medchemexpress.com/dspe-peg-2000.html.

[30] N. Wathoni et al. “Monoclonal antibody as a targeting mediator for nanoparticle targeted delivery system for lung cancer”. In: *Drug Delivery* 29.1 (2022), p. 2959. DOI: 10.1080/10717544.2022.2120566.

[31] L. Battaglia and M. Gallarate. “Lipid nanoparticles: state of the art, new preparation methods and challenges in drug delivery”. In: *Expert Opin. Drug Deliv.* (2012). URL: https://www.tandfonline.com/doi/full/10.1517/17425247.2012.673278.

[32] R. van der Meel et al. “Modular Lipid Nanoparticle Platform Technology for siRNA and Lipophilic Prodrug Delivery”. In: *Small* 17.37 (2021), p. 2103025. ISSN: 1613-6810. DOI: 10.1002/smll.202103025.

[33] R. Tenchov, R. Bird, A. E. Curtze, and Q. Zhou. “Lipid xn–NanoparticlesFrom-4k1l Liposomes to mRNA Vaccine Delivery, a Landscape of Research Diversity and Advancement”. In: *ACS Nano* 15.11 (2021), pp. 16982–17015. ISSN: 1936-0851. DOI: 10.1021/acsnano.1c04996.

[34] T.-T.-L. Nguyen and V.-A. Duong. “Solid Lipid Nanoparticles”. In: *Encyclopedia* 2.2 (2022), pp. 952–973. ISSN: 2673-8392. DOI: 10.3390/encyclopedia2020063.

[35] O. A. Madkhali. “Perspectives and Prospective on Solid Lipid Nanoparticles as Drug Delivery Systems”. In: *Molecules* 27.5 (2022). DOI: 10.3390/molecules27051543.

[36] M. Mehta, T. A. Bui, X. Yang, Y. Aksoy, E. M. Goldys, and W. Deng. “Lipid-Based Nanoparticles for Drug/Gene Delivery: An Overview of the Production Techniques and Difficulties Encountered in Their Industrial Development”. In: *ACS Mater. Au* 3.6 (2023), pp. 600–619. DOI: 10.1021/acsmaterialsau.3c00032.

[37] D. Irby, C. Du, and F. Li. “Lipid–Drug Conjugate for Enhancing Drug Delivery”. In: *Mol. Pharmaceutics* 14.5 (2017), p. 1325. DOI: 10.1021/acs.molpharmaceut.6b01027.

[38] S. Dadiboyena and A. Nefzi. “Synthesis of functionalized tetrasubstituted pyrazolyl heterocycles – A review”. In: *Eur. J. Med. Chem.* 46.11 (2011), pp. 5258–5275. ISSN: 0223-5234. DOI: 10.1016/j.ejmech.2011.09.016.

[39] K. Weiss, J. Racho, and J. Riemer. “Compartmentalized disulfide bond formation pathways”. In: *Redox Chemistry and Biology of Thiols*. Cambridge, MA, USA: Academic Press, 2022, pp. 321–340. ISBN: 978-0-323-90219-9. DOI: 10.1016/B978-0-323-90219-9.00020-0.

[40] D. Urimi et al. “Structural Characterization Study of a Lipid Nanocapsule Formulation Intended for Drug Delivery Applications Using Small-Angle Scattering Techniques”. In: *Mol. Pharmaceutics* 19.4 (2022), pp. 1068–1077. ISSN: 1543-8384. DOI: 10.1021/acs.molpharmaceut.1c00648.

[41] N. T. Huynh, C. Passirani, P. Saulnier, and J. P. Benoit. “Lipid nanocapsules: A new platform for nanomedicine”. In: *Int. J. Pharm.* 379.2 (2009), pp. 201–209. ISSN: 0378-5173. DOI: 10.1016/j.ijpharm.2009.04.026.

[42] P. Kumar et al. “Lipid Nanocapsule: A Novel Approach to Drug Delivery System Formulation Development”. In: *Current Pharm. Biotechnol.* 25.3 (2024), pp. 268–284. ISSN: 1873-4316. DOI: 10.2174/1389201024666230523114350. eprint: 37231750.

[43] J. Yoo, C. Park, G. Yi, D. Lee, and H. Koo. “Active Targeting Strategies Using Biological Ligands for Nanoparticle Drug Delivery Systems”. In: *Cancers* 11.5 (2019). DOI: 10.3390/cancers11050640.

[44] F. Salahpour Anarjan. “Active targeting drug delivery nanocarriers: Ligands”. In: *Nano-Structures & Nano-Objects* 19 (2019), p. 100370. ISSN: 2352-507X. DOI: 10.1016/j.nanoso.2019.100370.

[45] L. Malavolta and F. R. Cabral. “Peptides: Important tools for the treatment of central nervous system disorders”. In: *Neuropeptides* 45.5 (2011), pp. 309–316. ISSN: 0143-4179. DOI: 10.1016/j.npep.2011.03.001.

[46] C. Fu, L. Yu, Y. Miao, X. Liu, Z. Yu, and M. Wei. “Peptide–drug conjugates (PDCs): a novel trend of research and development on targeted therapy, hype or hope?” In: *Acta Pharmaceutica Sinica. B* 13.2 (2023), p. 498. DOI: 10.1016/j.apsb.2022.07.020.

[47] N. Yadav et al. “Polysaccharide-Drug Conjugates: A Tool for Enhanced Cancer Therapy”. In: *Polymers* 14.5 (2022). DOI: 10.3390/polym14050950.

[48] S. S. Panikar, N. Banu, J. Haramati, S. del Toro-Arreola, A. Riera Leal, and P. Salas. “Nanobodies as efficient drug-carriers: Progress and trends in chemotherapy”. In: *J. Controlled Release* 334 (2021), pp. 389–412. ISSN: 0168-3659. DOI: 10.1016/j.jconrel.2021.05.004.

[49] Y. Hu, C. Liu, and S. Muyldermans. “Nanobody-Based Delivery Systems for Diagnosis and Targeted Tumor Therapy”. In: *Front. Immunol.* 8 (2017). DOI: 10.3389/fimmu.2017.01442.

[50] P. S. Kozani, P. S. Kozani, and F. Rahbarizadeh. “The Potential Applicability of Single-Domain Antibodies (VHH): From Checkpoint Blockade to Infectious Disease Therapy”. In: *J. Adv. Immunopharmacol.* 1.2 (2021). ISSN: 2950-5461. DOI: 10.5812/tms.114888.

[51] A. K. Mehata, D. Dehari, Vikas, V. Priya, and M. S. Muthu. “Drug-releasing textile materials: current developments and future perspectives”. In: *Fiber and Textile Engineering in Drug Delivery Systems*. Buckingham, England, UK: Woodhead Publishing, 2023, pp. 1–38. ISBN: 978-0-323-96117-2. DOI: 10.1016/B978-0-323-96117-2.00001-7.

[52] J. Skopinska-Wisniewska, S. De la Flor, and J. Kozlowska. “From Supramolecular Hydrogels to Multifunctional Carriers for Biologically Active Substances”. In: *Int. J. Mol. Sci.* 22.14 (2021), p. 7402. ISSN: 1422-0067. DOI: 10.3390/ijms22147402.

[53] E. Seyrek and G. Decher. “7.09 - Layer-by-Layer Assembly of Multifunctional Hybrid Materials and Nanoscale Devices”. In: *Polymer Science: A Comprehensive Reference*. Vol. 7. Walthm, MA, USA: Elsevier, Jan. 2012, pp. 159–185. ISBN: 978-0-08-087862-1. DOI: 10.1016/B978-0-444-53349-4.00182-5.

[54] R. Sheyi, B. G. de la Torre, and F. Albericio. “Linkers: An Assurance for Controlled Delivery of Antibody-Drug Conjugate”. In: *Pharmaceutics* 14.2 (2022). DOI: 10.3390/pharmaceutics14020396.

[55] D. Motiejunas and R. C. Wade. “4.09 - Structural, Energetic, and Dynamic Aspects of Ligand–Receptor Interactions”. In: *Comprehensive Medicinal Chemistry II*. Vol. 4. Walthm, MA, USA: Elsevier, Jan. 2007, pp. 193–213. ISBN: 978-0-08-045044-5. DOI: 10.1016/B0-08-045044-X/00250-9.

[56] Q. Sun. “The Hydrophobic Effects: Our Current Understanding”. In: *Molecules* 27.20 (2022). DOI: 10.3390/molecules27207009.

[57] C. E. Chivers, A. L. Koner, E. D. Lowe, and M. Howarth. “How the biotin–streptavidin interaction was made even stronger: investigation via crystallography and a chimaeric tetramer”. In: *Biochem. J.* 435.Pt 1 (2011), p. 55. DOI: 10.1042/BJ20101593.

[58] S. Belbekhouche, M. Guerrouache, and B. Carbonnier. “Thiol–Maleimide Michael Addition Click Reaction: A New Route to Surface Modification of Porous Polymeric Monolith”. In: *Macromol. Chem. Phys.* 217.8 (2016), pp. 997–1006. ISSN: 1022-1352. DOI: 10.1002/macp.201500427.

[59] L. Martínez-Jothar et al. “Insights into maleimide-thiol conjugation chemistry: Conditions for efficient surface functionalization of nanoparticles for receptor targeting”. In: *J. Controlled Release* 282 (2018), pp. 101–109. ISSN: 0168-3659. DOI: 10.1016/j.jconrel.2018.03.002.

[60] N. Z. Fantoni, A. H. El-Sagheer, and T. Brown. “A Hitchhiker’s Guide to Click-Chemistry with Nucleic Acids”. In: *Chem. Rev.* 121.12 (2021), pp. 7122–7154. ISSN: 0009-2665. DOI: 10.1021/acs.chemrev.0c00928.

[61] M. Meldal and C. W. Tornøe. “Cu-Catalyzed Azide-Alkyne Cycloaddition”. In: *Chem. Rev.* 108.8 (2008), pp. 2952–3015. ISSN: 0009-2665. DOI: 10.1021/cr0783479.

[62] E. T. DiMartini, K. Kyker-Snowman, and D. I. Shreiber. “A click chemistry-based, free radical-initiated delivery system for the capture and release of payloads”. In: *Drug Delivery* 30.1 (2023). DOI: 10.1080/10717544.2023.2232952.

[63] *Click Chemistry Reactions: CuAAC, SPAAC, Diels-Alder | Biopharma PEG*. [Online; accessed 14. May 2024]. May 2024. URL: https://www.biochempeg.com/article/71.html.

[64] A. Zielińska et al. “Polymeric Nanoparticles: Production, Characterization, Toxicology and Ecotoxicology”. In: *Molecules* 25.16 (2020). DOI: 10.3390/molecules25163731.

[65] M. Danaei et al. “Impact of Particle Size and Polydispersity Index on the Clinical Applications of Lipidic Nanocarrier Systems”. In: *Pharmaceutics* 10.2 (2018). DOI: 10.3390/pharmaceutics10020057.

[66] S. K. Brar and M. Verma. “Measurement of nanoparticles by light-scattering techniques”. In: *TrAC, Trends Anal. Chem.* 30.1 (2011), pp. 4–17. ISSN: 0165-9936. DOI: 10.1016/j.trac.2010.08.008.

[67] S. Bhattacharjee. “DLS and zeta potential – What they are and what they are not?” In: *J. Controlled Release* 235 (2016), pp. 337–351. ISSN: 0168-3659. DOI: 10.1016/j.jconrel.2016.06.017.

[68] *Scanning Electron Microscope - Environmental Health and Safety - Purdue University*. [Online; accessed 5. May 2024]. Feb. 2024. URL: https://www.purdue.edu/ehps/rem/laboratory/equipment%20safety/Research%20Equipment/sem.html.

[69] A. B. Nowakowski, W. J. Wobig, and D. H. Petering. “Native SDS-PAGE: High Resolution Electrophoretic Separation of Proteins With Retention of Native Properties Including Bound Metal Ions”. In: *Metallomics : integrated biometal science* 6.5 (2014), p. 1068. DOI: 10.1039/c4mt00033a.

[70] K. Gavini and K. Parameshwaran. “Western Blot”. In: *StatPearls [Internet]*. StatPearls Publishing, Apr. 2023. URL: https://www.ncbi.nlm.nih.gov/books/NBK542290.

[71] T. Mahmood and P.-C. Yang. “Western Blot: Technique, Theory, and Trouble Shooting”. In: *North American Journal of Medical Sciences* 4.9 (2012), p. 429. DOI: 10.4103/1947-2714.100998.

[72] *DTT (dithiothreitol)*. [Online; accessed 9. Jul. 2024]. July 2024. URL: https://www.thermofisher.com/order/catalog/product/R0861.

[73] *3-Azido-1-propanol*. [Online; accessed 9. Jul. 2024]. July 2024. URL: https://www.sigmaaldrich.com/NL/en/product/aldrich/776130.

[74] *FITC-PEG-SH*. [Online; accessed 9. Jul. 2024]. July 2024. URL: https://www.biochempeg.com/product/FITC-PEG-SH.html.

[75] P. Gupta, N. Rai, A. Verma, and V. Gautam. “Microscopy based methods for characterization, drug delivery, and understanding the dynamics of nanoparticles”. In: *Med. Res. Rev.* 44.1 (2024), pp. 138–168. ISSN: 0198-6325. DOI: 10.1002/med.21981.

[76] J. Gross, S. Sayle, A. R. Karow, U. Bakowsky, and P. Garidel. “Nanoparticle tracking analysis of particle size and concentration detection in suspensions of polymer and protein samples: Influence of experimental and data evaluation parameters”. In: *Eur. J. Pharm. Biopharm.* 104:30-41. (2016). ISSN: 1873-3441. DOI: 10.1016/j.ejpb.2016.04.013. eprint: 27108267.

[77] [Online; accessed 8. Jul. 2024]. July 2024. URL: https://ris.utwente.nl/ws/portalfiles/portal/354731225/ENZYME_RESPONSIVE_DELIVERY_OF_ENGINEERED_.pdf.

[78] E. A. Berg and J. B. Fishman. “Labeling Antibodies Using N-Hydroxysuccinimide (NHS)-Fluorescein”. In: *Cold Spring Harb. Protoc.* 2019.3 (2019), p. . ISSN: 1559-6095. DOI: 10.1101/pdb.prot099283. eprint: 30824621.

[79] *Why is Replication in Research Important? | AJE*. [Online; accessed 10. Jul. 2024]. July 2024. URL: https://www.aje.com/arc/why-is-replication-in-research-important.

Appendix A

Inconclusive results

A.1 Post-insertion DSPE-PEG-Mal-Cy3

The post-insertion experiment was performed once with DSPE-PEG-Mal-Cy3 into LNPs, the result can be seen in figure A.1. The Cy3 fluorescence of the lipids is shown in figure A.1a. The sample with LNPs shows Cy3 fluorescence, which is not as expected since there are no DSPE-PEG-Mal-Cy3 in the sample to be detected. The Cy5.5 fluorescence of the LNPs can be seen in figure A.1b. The sample with only DSPE-PEG-Mal-Cy3 with 5000 Da PEG 0.2% shows Cy5.5 fluorescence, which is not as expected since there should be no LNPs with Cy5.5 fluorescence present in the sample. During freeze-drying of all the samples after post-insertion, cross-contamination took place. This means that all the samples are mixed and the results are inconclusive.

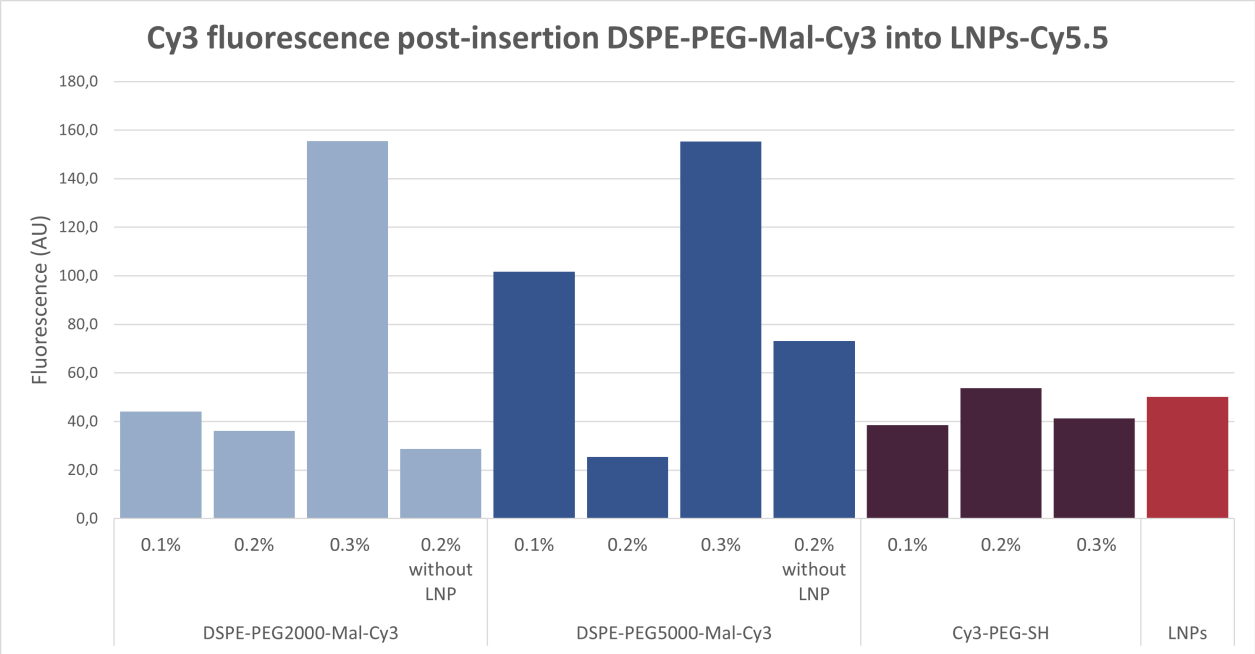

(a)

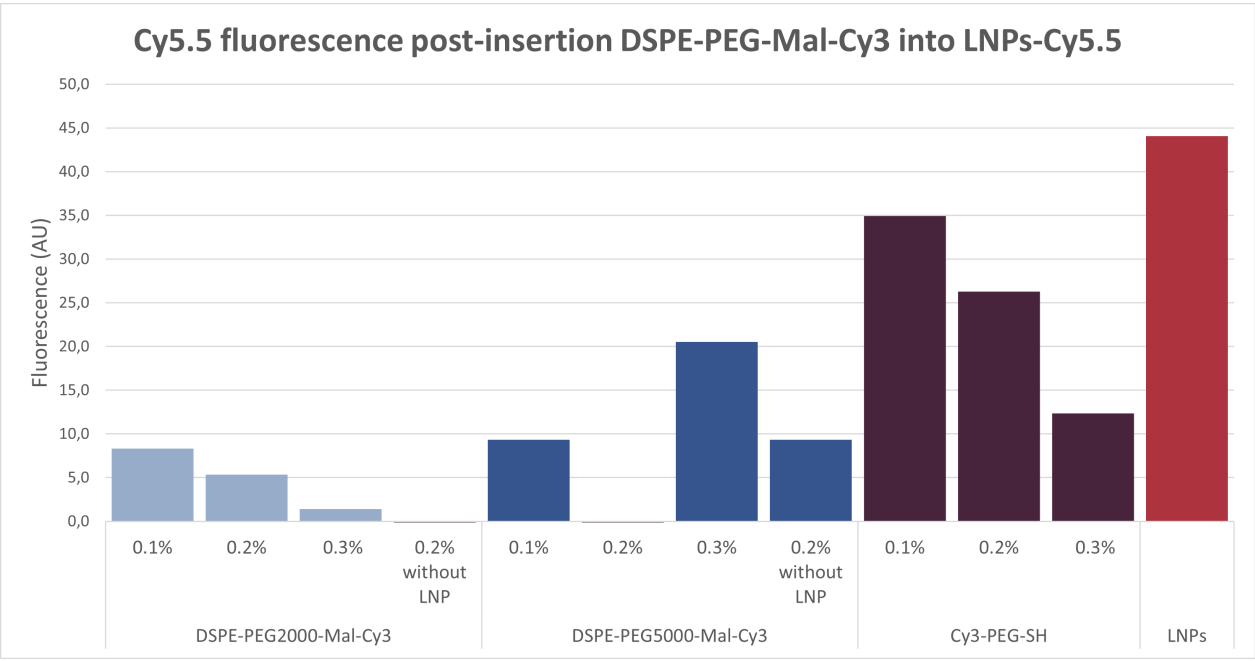

(b)

Figure A.1: The fluorescence results of the post-insertion with lipids-Mal-Cy3 into LNPs. No standard deviation is shown since the measurements are performed once. (a) The Cy3 fluorescence of the lipids. (b) The Cy5.5 fluorescence of the LNPs.

The DLS data was measured before freeze-drying, the cross-contamination did not occur yet. Table A.1 shows the results from the DLS measurements, with the hydrodynamic size and the PDI of the LNPs. Figure A.2 visualizes these results. The LNPs without any post-insertion have a diameter of 112.3 $\pm$ 0.82 nm and a PDI of 0.138. LNPs with Cy3-PEG-SH (as control, without lipids) added in three different molar ratios show a similar size, but a slightly bigger PDI. LNPs with post-inserted with DSPE-PEG-Mal-Cy3 with 2000 Da PEG 0.1 % and 0.2% molarity show a small increase in size while the PDI doubles/increases compared to the LNPs without post-insertion. LNPs post-inserted with DSPE-PEG-Mal-Cy3 with 5000 Da PEG show in general much larger sizes, compared to the post-insertion of equivalent 2000 Da PEG lipids. The LNPs post-inserted with 0.3 % DSPE-PEG-Mal-Cy3 show a size of above 1000 nm for both PEG lengths. The PDI

of these samples are for both also very high, with a value of almost 1.

Table A.1: The hydrodynamic size and PDI of the LNPs made with post-insertion of DSPE-PEG-Mal-Cy3 lipids measured with DLS, the Z-average (nm) is shown.

	Hydrodynamic size (nm)	**Polydispersity Index (PDI)**
LNP	112.3 ± 0.82	0.138
LNP DSPE-PEG2k-Mal-Cy3 0.1%	134.5 ± 9.82	0.331
LNP DSPE-PEG2k-Mal-Cy3 0.2%	120.2 ± 12.10	0.232
LNP DSPE-PEG2k-Mal-Cy3 0.3%	2002 ± 276.15	1
LNP DSPE-PEG5k-Mal-Cy3 0.1%	846.9 ± 301.63	0.692
LNP DSPE-PEG5k-Mal-Cy3 0.2%	369.9 ± 307.98	0.861
LNP DSPE-PEG5k-Mal-Cy3 0.3%	3039.3 ± 828.35	0.784
LNP Cy3 0.1 %	105.4 ± 1.87	0.184
LNP Cy3 0.2 %	128.6 ± 3.04	0.205
LNP Cy3 0.3 %	116.1 ± 6.07	0.229

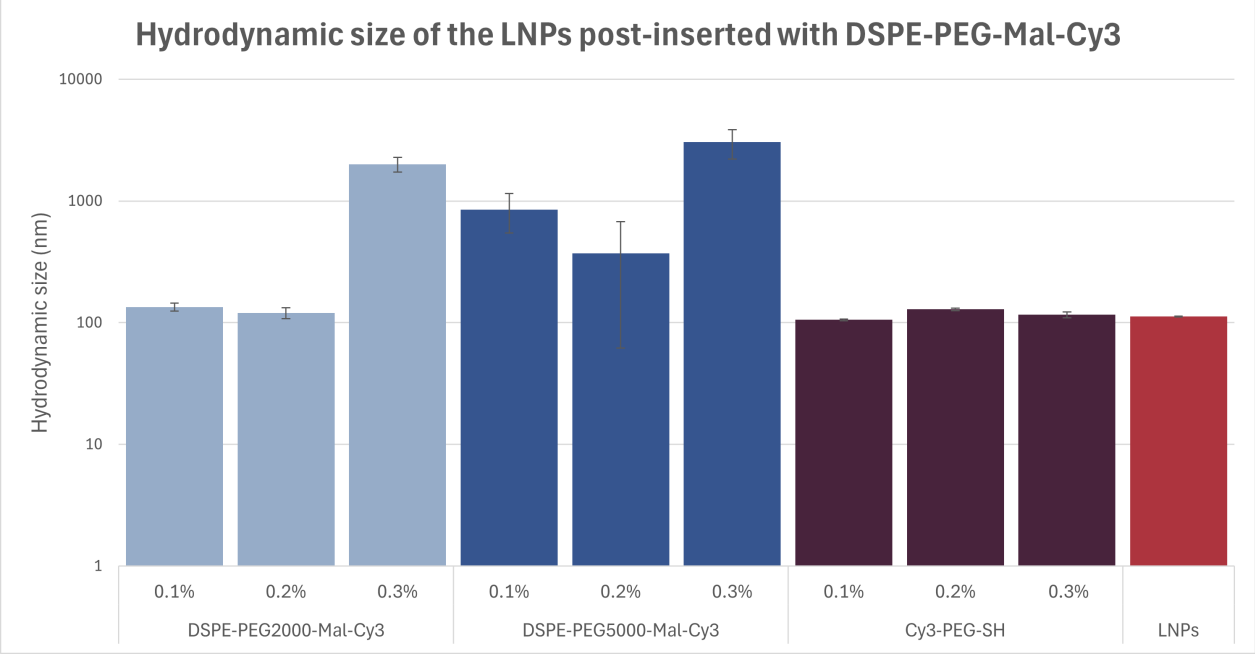

Figure A.2: The hydrodynamic size of the LNPs post-inserted with Mal-Cy3 lipids, with values from table A.1. The values are shown on a logarithmic scale.

A.2 Post-insertion DSPE-PEG-DBCO-Cy3 batch 1

The post-insertion experiment was performed with DSPE-PEG-DBCO-Cy3 into LNPs. The first batch of the post-insertion is inconclusive and is discussed below in this section. The protocol for this experiment was optimized and the experiment was performed in total three times, the results of these experiments can be seen in section 4.4. Three molar ratios are tested: 0.1, 0.2 and 0.3 %. Three controls are taken into consideration, a sample without LNPs, without DSPE-PEG-Mal-Cy3 and lastly a sample with only Cy3-PEG-SH and LNPs.

Figure A.3 shows the fluorescence results of the post-insertion. In figure A.3a, the Cy3 fluorescence of DSPE-PEG-DBCO-Cy3 can be seen. There is (almost)no fluorescence for DSPE-PEG-DBCO with 2000 Da PEG. DSPE-PEG-DBCO-CY3 with 5000 Da PEG show a high fluorescence value. The control with only Cy3-PEG-SH dye shows a relatively high fluorescence, this means that not all the free dye is dialyzed out

of the membranes or non-specific binding of Cy3-PEG-SH to the LNPs took place. The control sample with only LNPs and the sample with only DSPE-PEG-DBCO-Cy3 with 2000 Da PEG show both no fluorescence, as expected. However, the control with only DSPE-PEG-DBCO-Cy3 with 5000 Da PEG shows a high fluorescence, this could be because the DLS measures faulty or DSPE-PEG-DBCO-Cy3 forms micelles, these are not filtered out of the dialysis membranes.

The Cy5.5 fluorescence can be seen in figure A.3b. The amount of Cy5.5 is fluctuating for every sample. The control samples with only DSPE-PEG-DBCO-Cy3 show no Cy5.5 fluorescence, as expected. The Cy3/Cy5,5 values can be seen in figure A.3c, averaged out for the difference in number of particles present in the samples. The post-inserted DSPE-PEG-DBCO-Cy3 with 2000 Da PEG shows almost a value of 0. The post-inserted DSPE-PEG-DBCO-Cy3 with 5000 Da PEG show higher values, with an increase in fluorescence with an increase in molar ratio of the lipid. The control group with only LNPs show a value of 0, as expected. The control groups with only Cy3-PEG-SH dye added to the LNPs show higher values than the post-inserted LNPs. This is not as expected, the reasons for this could be the hydrophobic non-specific binding of the Cy3-PEG-SH dye to the LNPs.

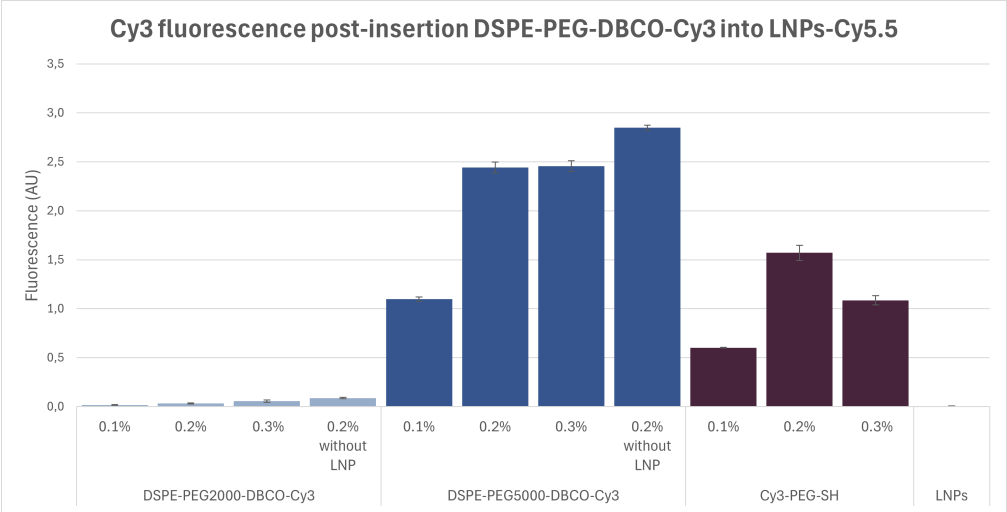

(a)

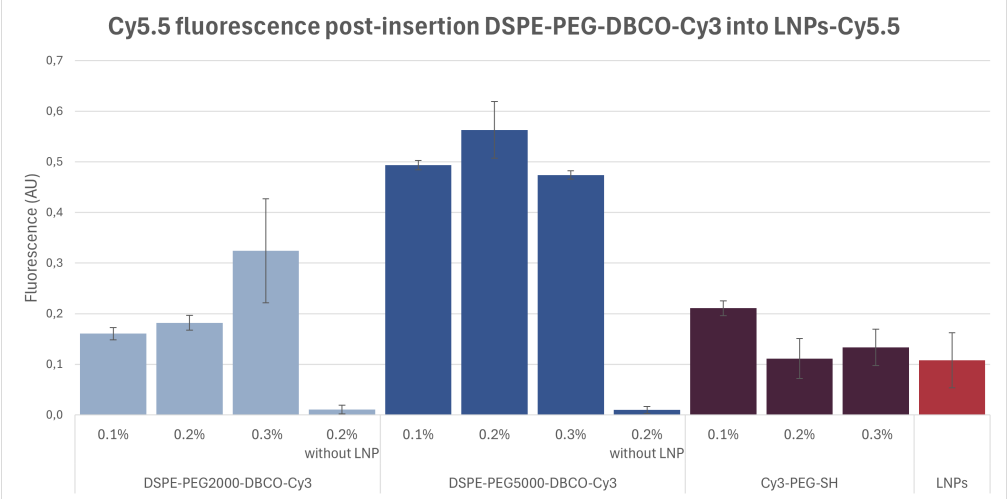

(b)

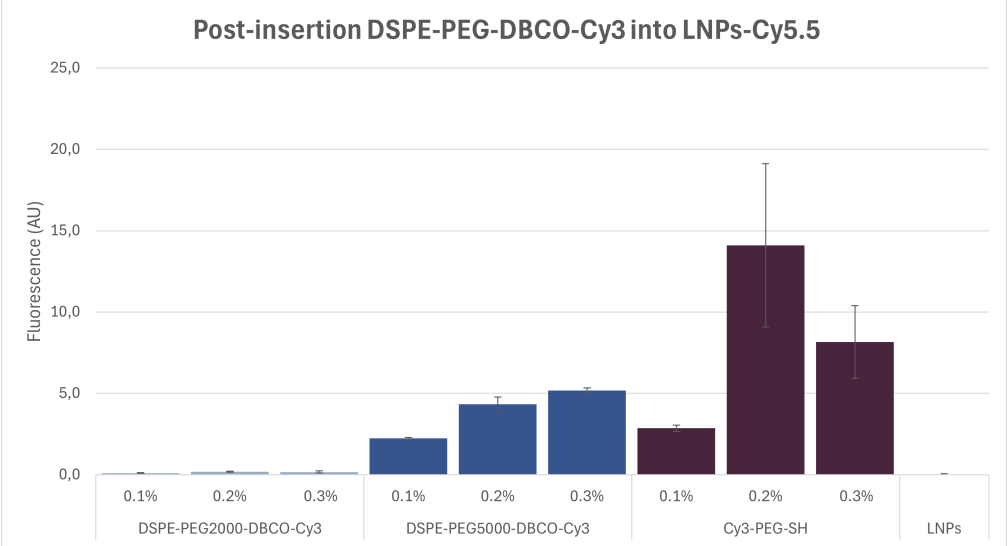

(c)

Figure A.3: The fluorescence results of the post-insertion with DSPE-PEG-DBCO-Cy3 into the LNPs of batch 1. (a) The Cy3 fluorescence of DSPE-PEG-DBCO-Cy3. (b) The Cy5.5 fluorescence of the LNPs, sample with Cy3 dye 0.3% has fewer LNPs added. (c) Averaged out values are Cy3 values divided by Cy5.5 values to average out the difference in the number of particles present in each sample.

The DLS data of the post-insertion with DSPE-PEG-DBCO-Cy3 is shown in table A.2 and visualized in figure A.4. The sample with only LNPs has a size of 239.1 ± 20.3 with a PDI of 0.306. The samples with only Cy3-PEG-SH show a small increase in size of approximately 100 nm and an increase in the PDI of approximately 0.1. This could imply that DSPE-PEG-DBCO-Cy3 binds non-specific to the LNPs. All molar ratios of the post-inserted DSPE-PEG-DBCO-Cy3 with 2000 Da PEG show an increase in size, compared to the LNPs without post-insertion. The molar ratio of 0.1 % shows the smallest increase in size and the lowest PDI of the three molar ratios. The molar ratio of 0.2 % shows the biggest increase in size, but also the highest PDI of 0.646. All molar ratios of the post-insertion with DSPE-PEG-DBCO-Cy3 with 5000 Da PEG show in general an increase in size, compared to the sample with only LNPs. Except, the molar ratio of 0.2 % shows a small decrease in size. The molar ratio of 0.3 % shows the smallest increase in size. The PDIs of the LNPs increased by approximately 0.1, the PDI is about the same for every post-insertion with DSPE-PEG-DBCO-Cy3 with 5000 Da PEG. The samples with Cy3-PEG-SH added in the three molar ratios show an increase in size and PDI. The increase in size is only tens of nms and the PDI increases by approximately 0.1.

Table A.2: The hydrodynamic size and PDI of the LNPs made with post-insertion of DSPE-PEG-DBCO-Cy3 lipids batch 1 measured with DLS, the Z-average (nm) is shown.

	Hydrodynamic size (nm)	**Polydispersity Index (PDI)**
LNP	239.1 ± 20.3	0.306
LNP DSPE-PEG2000-DBCO-Cy3 0.1%	403.9 ± 31.1	0.454
LNP DSPE-PEG2000-DBCO-Cy3 0.2%	638.1 ± 76.6	0.646
LNP DSPE-PEG2000-DBCO-Cy3 0.3%	467.4 ± 165.0	0.481
LNP DSPE-PEG5000-DBCO-Cy3 0.1%	448.5 ± 34.6	0.415
LNP DSPE-PEG5000-DBCO-Cy3 0.2%	222.4 ± 3.5	0.410
LNP DSPE-PEG5000-DBCO-Cy3 0.3%	302.0 ± 51.1	0.445
LNP Cy3-PEG-SH 0.1 %	292.6 ± 65.3	0.387
LNP Cy3-PEG-SH 0.2 %	389.3 ± 162.8	0.487
LNP Cy3-PEG-SH 0.3 %	271.5 ± 73.5	0.485

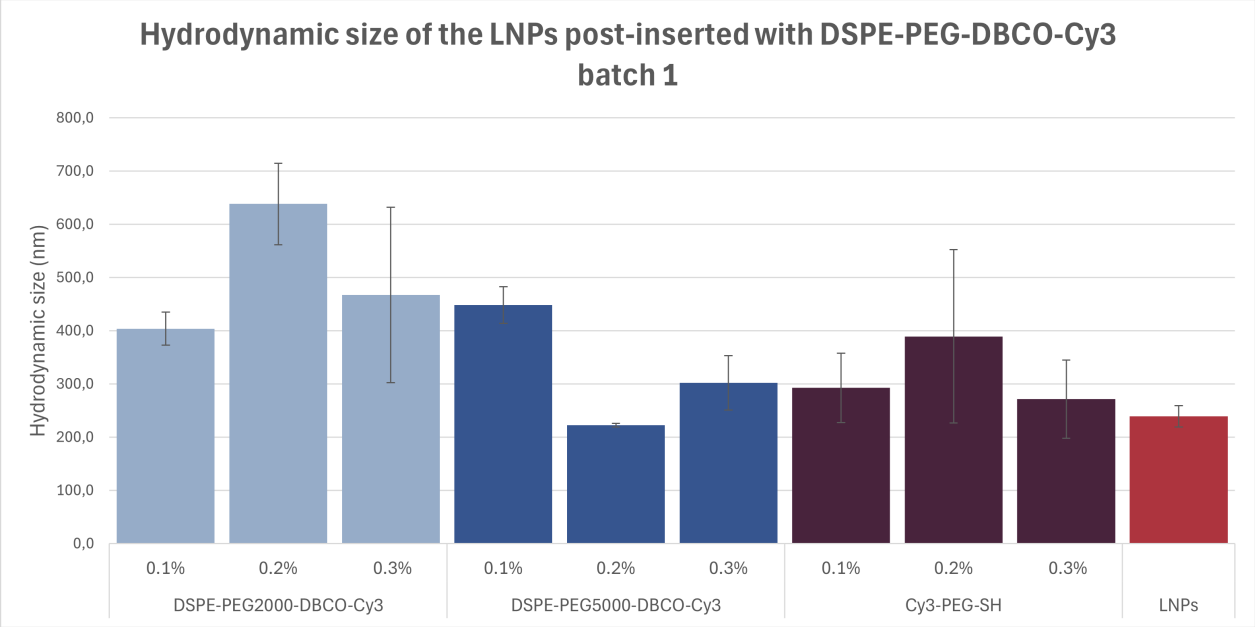

Figure A.4: The hydrodynamic size of the LNPs post-inserted with DSPE-PEG-DBCO-Cy3 of batch 1, with values from table A.2.